

# NAVAL POSTGRADUATE SCHOOL

## Monterey, California



## THESIS

### DEEP MIXED LAYER ENTRAINMENT

by

Rebecca E. Stone

March, 1997

Thesis Co-Advisors:      Roland W. Garwood, Jr.  
Peter S. Guest

Approved for public release; distribution is unlimited.

DTIC QUALITY INSPECTED 4

19971201 064

REPORT DOCUMENTATION PAGE			Form Approved OMB No. 0704-0188	
Public reporting burden for this collection of information is estimated to average 1 hour per response, including the time for reviewing instruction, searching existing data sources, gathering and maintaining the data needed, and completing and reviewing the collection of information. Send comments regarding this burden estimate or any other aspect of this collection of information, including suggestions for reducing this burden, to Washington Headquarters Services, Directorate for Information Operations and Reports, 1215 Jefferson Davis Highway, Suite 1204, Arlington, VA 22202-4302, and to the Office of Management and Budget, Paperwork Reduction Project (0704-0188) Washington DC 20503.				
1. AGENCY USE ONLY (Leave blank)		2. REPORT DATE MARCH 97		3. REPORT TYPE AND DATES COVERED Master's Thesis
4. TITLE AND SUBTITLE DEEP MIXED LAYER ENTRAINMENT			5. FUNDING NUMBERS	
6. AUTHOR(S) Rebecca E. Stone				
7. PERFORMING ORGANIZATION NAME(S) AND ADDRESS(ES) Naval Postgraduate School Monterey CA 93943-5000			8. PERFORMING ORGANIZATION REPORT NUMBER	
9. SPONSORING/MONITORING AGENCY NAME(S) AND ADDRESS(ES)			10. SPONSORING/MONITORING AGENCY REPORT NUMBER	
11. SUPPLEMENTARY NOTES The views expressed in this thesis are those of the author and do not reflect the official policy or position of the Department of Defense or the U.S. Government.				
12a. DISTRIBUTION/AVAILABILITY STATEMENT Approved for public release; distribution is unlimited.			12b. DISTRIBUTION CODE	
13. ABSTRACT (maximum 200 words) A bulk turbulence-closure mixed layer model is generalized to allow prediction of very deep polar sea mixing. The model includes unsteady three-component turbulent kinetic energy budgets. In addition to terms for shear production, pressure redistribution, and dissipation, special attention is devoted to realistic treatment of thermobaric enhancement of buoyancy flux and to Coriolis effects on turbulence. The model is initialized and verified with CTD data taken by R/V Valdivia in the Greenland Sea during winter 1993-1994. Model simulations show (i) mixed layer deepening is significantly enhanced when the thermal expansion coefficient's increase with pressure is included; (ii) entrainment rate is sensitive to the direction of wind stress because of Coriolis; and (iii) the predicted mixed layer depth evolution agrees qualitatively with the observations. Results demonstrate the importance of water column initial conditions, accurate representation of strong surface cooling events, and inclusion of the thermobaric effect on buoyancy, to determine the depth of mixing and ultimately the heat and salt flux into the deep ocean. Since coupling of the ocean to the atmosphere through deep mixed layers in polar regions is fundamental to our climate system, it is important that regional and global models be developed that incorporate realistic representation of this coupling.				
14. SUBJECT TERMS Ocean Mixed Layer Polar Oceans Deep Entrainment			15. NUMBER OF PAGES 78	
			16. PRICE CODE	
17. SECURITY CLASSIFICATION OF REPORT Unclassified	18. SECURITY CLASSIFICATION OF THIS PAGE Unclassified	19. SECURITY CLASSIFICATION OF ABSTRACT Unclassified	20. LIMITATION OF ABSTRACT UL	

NSN 7540-01-280-5500

Standard Form 298 (Rev. 2-89)  
Prescribed by ANSI Std. Z39-18 298-102



Approved for public release; distribution is unlimited.

**DEEP MIXED LAYER  
ENTRAINMENT**

Rebecca E. Stone  
Lieutenant Commander, United States Navy  
B.S., San Diego State University, 1985

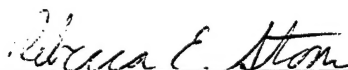
Submitted in partial fulfillment  
of the requirements for the degrees of

**MASTER OF SCIENCE IN METEOROLOGY  
MASTER OF SCIENCE IN PHYSICAL OCEANOGRAPHY**

from the

**NAVAL POSTGRADUATE SCHOOL  
March 1997**

Author:



Rebecca E. Stone

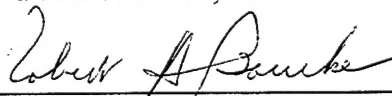
Approved by:



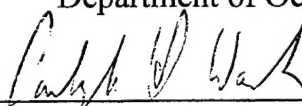
Roland W. Garwood, Jr., Thesis Co-Advisor



Peter S. Guest, Thesis Co-Advisor



Robert H. Bourke, Chairman  
Department of Oceanography



Carlyle H. Wash, Chairman  
Department of Meteorology



## ABSTRACT

A bulk turbulence-closure mixed layer model is generalized to allow prediction of very deep polar sea mixing. The model includes unsteady three-component turbulent kinetic energy budgets. In addition to terms for shear production, pressure redistribution, and dissipation, special attention is devoted to realistic treatment of thermobaric enhancement of buoyancy flux and to Coriolis effects on turbulence. The model is initialized and verified with CTD data taken by R/V Valdivia in the Greenland Sea during winter 1993-1994. Model simulations show (i) mixed layer deepening is significantly enhanced when the thermal expansion coefficient's increase with pressure is included; (ii) entrainment rate is sensitive to the direction of wind stress because of Coriolis; and (iii) the predicted mixed layer depth evolution agrees qualitatively with the observations. Results demonstrate the importance of water column initial conditions, accurate representation of strong surface cooling events, and inclusion of the thermobaric effect on buoyancy, to determine the depth of mixing and ultimately the heat and salt flux into the deep ocean. Since coupling of the ocean to the atmosphere through deep mixed layers in polar regions is fundamental to our climate system, it is important that regional and global models be developed that incorporate realistic representation of this coupling.



## TABLE OF CONTENTS

I. INTRODUCTION .....	1
A. BACKGROUND .....	1
B. OBJECTIVE .....	2
II. MIXED LAYER THEORY .....	5
A. GENERAL MIXED LAYER AND DEEP WATER FORMATION THEORY .....	5
B. THERMOBARICITY .....	6
C. ROTATION IN ATMOSPHERIC AND OCEANIC BOUNDARY LAYERS .....	7
III. MODEL .....	9
A. DERIVING THE EQUATIONS FOR TURBULENT KINETIC ENERGY .....	9
B. INTEGRATING FOR BULK TKE .....	12
C. TEMPERATURE AND SALINITY EQUATIONS .....	19
D. BULK MOMENTUM EQUATIONS .....	20
E. ENTRAINMENT VELOCITY .....	21
F. NUMERICAL APPROACH .....	23



IV. OBSERVATIONAL DATA .....	25
A. IMPORTANCE OF THE GREENLAND SEA REGION .....	25
B. OCEANOGRAPHIC DATA .....	26
C. METEOROLOGICAL DATA .....	29
V. MODEL RESULTS .....	33
A. EFFECT OF THERMOBARICITY .....	33
B. EFFECT OF COOLING .....	38
C. EFFECT OF $\Omega_2$ ROTATION .....	38
D. CONSTANT AVERAGE FORCING RESULTS COMPARED TO DATA .....	41
E. TIME DEPENDENT FORCING .....	41
VII. CONCLUSIONS .....	59
A. SUMMARY .....	59
B. RECOMMENDATIONS .....	60
LIST OF REFERENCES .....	63
INITIAL DISTRIBUTION LIST .....	65

## ACKNOWLEDGMENT

The Author would like to acknowledge the support of the Office of Naval Research, Code 322OM, and the National Science Foundation, Office of Polar Programs.

The Author would like to thank Professor R. W. Garwood, Jr., for encouraging my interest in this area of study, for his guidance in conducting the research, and for his infectious enthusiasm. I also thank Mr. Ramsey Harcourt for helping me so patiently (and often) when I became "stuck". I am deeply indebted to my husband, Joe, and my sister, Martha, whose loving support made it possible for me to focus on the completion of this work.



## I. INTRODUCTION

### A. BACKGROUND

All interaction of the atmosphere with the ocean must occur where the two fluids are in contact - that is, in the upper, fully turbulent layer of the ocean known as the mixed layer. This mixed layer is typically more buoyant than the water below, so that changes in the atmosphere are to some extent isolated from the deep ocean by the more buoyant layer. Exceptions to this general structure are in the polar ocean regions, where mixing may occur to great depths, or even to the bottom. This coupling of the ocean to the atmosphere through deep mixed layers in polar regions is fundamental to the initiation of the global thermohaline conveyor belt and to the earth's climate system.

Mixed layer modeling has historically used a linear dependence of density upon temperature, so that the thermal expansion coefficient is treated as a constant. This approximation is valid over much of the ocean, where mixed layers are typically shallow, but breaks down in the ocean regions where there are large excursions in mixed-layer depth and/or mixed-layer temperature. The equation of state for seawater shows that the dependence of density and buoyancy upon temperature is not simply linear; the thermal expansion coefficient varies with pressure, and does so most at temperatures near freezing (Garwood, 1991). The thermobaric effect on the stability of a water column is most significant then where nearby parcels - very cold and at depth - have strong contrast in their potential temperatures. This is a characteristic state common to deep mixed layers in the polar seas, where traditional mixed layer modeling has failed to predict realistic mixing and deep water formation.

Another common approximation that may not be valid for deep mixed layers is the neglect of planetary rotation's effects on turbulence. In more shallow mixed layers, this neglect is reasonable because the scale of the turbulence is much smaller than the distance over which the effects of rotation can be felt, the Rossby radius. However, in polar regions the Rossby radius is much reduced ( $\sim 1$  km). The scale of turbulent eddies is equivalent to the depth of mixing, so if deep mixing occurs ( $\sim 1$  km), the eddies are large enough to be affected by planetary rotation, and the effects need to be included in models of deep entrainment. Furthermore, the vector planetary rotation ( $\vec{\Omega} = \Omega_y \hat{e}_y + \Omega_z \hat{e}_z$ ) needs to be considered because of the three-dimensionality of turbulence.

## **B. OBJECTIVE**

Deep mixing is controlled by factors more complex than those of traditional mixed layer physics; the proper representation of non-linear buoyancy effects, energy-converting rotational effects, non-steady atmospheric forcing and water column initial conditions is critical to calculating the fluxes of heat, salinity, and tracers into the deep ocean. In this research a model was developed and tested that expands on traditional mixed layer modeling by adding the effects of thermobaricity and planetary rotation, that allows initialization with hydrographic data, and that forces the mixing with realistic meteorological time series of surface heat flux and wind stress. The goal is not just to compare the final mixed layer depth to that observed, but to see how the observed event is simulated in terms of relative contributions of energy and evolution in time.

Chapter II summarizes the state of the art leading up to this research. The model equations are developed in Chapter III, and the numerical approach is discussed. Chapter IV

presents the oceanographic data used to initialize and the meteorological data used to force the model. Chapter V shows model results for hypothetical cases with constant forcing, followed by results with time dependent forcing. Chapter VI summarizes the results of the research and makes conclusions and recommendations for further study.



## II. MIXED LAYER THEORY

### A. GENERAL MIXED LAYER AND DEEP WATER FORMATION THEORY

Mixed layer theory concerning normal mixing depths ( $<100$  m) has been well developed and is summarized by Zilitinkevich et al. (1979), Garwood (1979), and more recently by Large et al. (1994). However, none of these has direct application to very deep mixing (order 1 km and greater).

Early speculations that deep water is formed not just by drainage off continental shelves, but by convection in the open ocean, were made by Nansen (1912) for the Arctic and by Wüst (1928) for the Antarctic; it was not until much later that there was enough evidence to prove that open ocean deep convection does occur.

Brown and Beardsley (1978) suggested that overturning during winter storms could be the primary source of mixing that forms Gulf of Maine Intermediate Water. They were cautious at the time, however, because they felt their data did not completely prove this result.

Gordon (1978) reported the discovery of a very localized region ( $\sim 13$  km) of convection in the Weddell Sea. Killworth (1979) showed that the entire region of the Weddell Sea gyre was susceptible to overturning, and that reduced stratification within cyclonic eddies could be the mechanism that "selects" such narrow areas of convection within the larger gyre.



## B. THERMOBARICITY

Gill (1973), considering the mixing of water flowing off the continental shelf into the Weddell Sea, noted the importance of the variation of the thermal expansion coefficient with depth in cold water. He included this effect in his calculations and determined that there could be parcels of water with potential temperature - salinity ( $\theta - s$ ) properties such that, if displaced a finite distance downward, the parcels would be unstable, their relative density to the surrounding water continuing to increase as they descended, thus accelerating the parcels downward.

McDougall (1987) coined the term thermobaricity for the increase in seawater's thermal expansion coefficient with pressure ( $p$ ), or the  $\frac{\partial}{\partial p} \left( \frac{\partial p}{\partial \theta} \right)$  term in the equation of state, investigated its effect on mixing across neutral surfaces, and discovered that although both upward and downward vertical velocities across the neutral surface are possible, they are usually downward.

Garwood (1991) studied thermobaricity's effect on mixing across a non-neutral surface, the interface at the bottom of the mixed layer. Although previously neglected, the buoyancy-flux enhancement by thermobaricity was found to be an important source of vertical turbulent kinetic energy, leading to increased entrainment.

Garwood et al. (1994) noted that in addition to enhancing entrainment rates, thermobaricity might assist in bringing surface water to depth by causing water column instabilities. A parcel-type instability would occur when a parcel from the cold and fresh turbulent layer overshoots the interface, and continues to accelerate downward because pressure compresses it more than the surrounding water is compressed. A layer-type

instability would occur as an interface advected downward becomes unstable due to the thermobaric effect.

### C. ROTATION IN ATMOSPHERIC AND OCEANIC BOUNDARY LAYERS

Rossby and Montgomery (1935) were the first to suggest that geophysical boundary layers should scale vertically with  $\frac{u_*}{f}$ , where  $u_*$  is the friction velocity and  $f = 2\Omega_3$  is the vertical component of planetary rotation. Hence a boundary layer "Rossby number" is  $\frac{u_*}{h f} \sim 1$ .

Gascard (1973) showed that in a homogeneous water column, large amplitude internal waves generated by wind surges in shallow regions can propagate upward because of planetary rotation, bringing energy with them, and suggested they may couple with  $\Omega$  and be involved in mixing and deep water formation.

Wyngaard et al. (1974) were the first to evaluate turbulence terms containing  $\Omega_2$ ; their study was of the convective atmospheric boundary layer, and found  $\Omega_2$ 's effect to be small. However, turning to ocean turbulence, Garwood (1977) found a Rossby number dependence for oceanic mixed layers in a bulk turbulence closure model. Garwood et al. (1985) went on to show that planetary rotation acts to exchange turbulent kinetic energy between horizontal and vertical components in a steady-state mixed layer. Vertical turbulent energy and thus mixed layer depth are increased under easterly winds. Garwood (1991) extended this hypothesis to the more general case of deepening mixed layers.



### III. MODEL

#### A. DERIVING THE EQUATIONS FOR TURBULENT KINETIC ENERGY

Representing the Navier-Stokes equations of motion as

$$\frac{\partial u_i}{\partial t} = -u_j \frac{\partial u_i}{\partial x_j} - \frac{1}{\rho} \frac{\partial p}{\partial x_i} - 2\epsilon_{ijk}\Omega_j u_k - \delta_{i3}g + \nu \frac{\partial^2 u_i}{\partial x_j^2} \quad (1)$$

the quantity turbulent kinetic energy is formed by decomposing the variables into their mean and turbulent parts, for example, representing one of the three velocity components as

$$u_i = \overline{u_i} + u_i' \quad (2)$$

where the turbulent part is not assumed to be small compared to the mean. Here  $i = 1, 2, 3$  corresponds to the Cartesian coordinate directions of east, north, and up;  $[\Omega_i] = \Omega [0 \cos \phi \sin \phi]$ ; molecular viscosity is  $\nu$ ; gravitational acceleration is  $g$ ; and  $\phi$  is latitude. The u-component kinetic energy per unit mass contained in the turbulence will then be

$$u_1 \text{ TKE} = \frac{\overline{u_1'^2}}{2} \quad (3)$$

Since

$$\frac{\partial}{\partial t} \left( \frac{\overline{u_1'^2}}{2} \right) = \overline{u_1' \frac{\partial u_1'}{\partial t}} - \overline{u_1' \frac{\partial u_1}{\partial t}} \quad (4)$$

and the right-hand-side contains only quantities predicted by the equations of motion, kinetic energy can be calculated. Again generalizing to the three components, the last term can be

written as

$$\begin{aligned} \overline{u_i \frac{\partial \overline{u_i}}{\partial t}} = & - \overline{u_i} \overline{u_j} \frac{\partial \overline{u_i}}{\partial x_j} - \overline{u_i u_j' \frac{\partial u_i'}{\partial x_j}} - \overline{u_i} \frac{1}{\rho_0} \frac{\partial \overline{p}}{\partial x_i} \\ & + \nu \overline{u_i} \frac{\partial^2 \overline{u_i}}{\partial x_j^2} - 2 \epsilon_{ijk} \Omega_j \overline{u_i} \overline{u_k} - \delta_{i3} \frac{g}{\rho_0} \overline{u_i} \overline{\rho} \end{aligned} \quad (5)$$

after Reynolds' decomposing, averaging, and making the Boussinesq approximation on equation (1). The first term on the right-hand-side of equation (4) is formed by performing the multiplication and decomposition first, and then averaging, resulting in

$$\begin{aligned} \overline{u_i \frac{\partial u_i}{\partial t}} = & - \overline{u_i} \overline{u_j} \frac{\partial \overline{u_i}}{\partial x_j} - \overline{u_i u_j' \frac{\partial u_i'}{\partial x_j}} - \overline{u_j} \frac{\partial \overline{u_i u_j'}}{\partial x_j} - \frac{\partial \overline{u_i}}{\partial x_j} \overline{u_i' u_j'} - \overline{u_i' u_j' \frac{\partial u_i'}{\partial x_j}} \\ & - \frac{1}{\rho_0} \overline{u_i} \frac{\partial \overline{p}}{\partial x_i} - \frac{1}{\rho_0} \overline{u_i' \frac{\partial p'}{\partial x_i}} + \nu \left( \overline{u_i} \frac{\partial^2 \overline{u_i}}{\partial x_j^2} + \overline{u_i' \frac{\partial^2 u_i'}{\partial x_j^2}} \right) \\ & - 2 \epsilon_{ijk} \Omega_j \left( \overline{u_i} \overline{u_k} + \overline{u_i' u_k'} \right) - \delta_{i3} \frac{g}{\rho_0} \left( \overline{u_i} \overline{\rho} - \overline{u_i' \rho'} \right) \end{aligned} \quad (6)$$

Subtracting, we have

$$\begin{aligned} \frac{1}{2} \frac{\partial \overline{u_i'^2}}{\partial t} = & - \overline{u_j} \overline{u_i' \frac{\partial u_i'}{\partial x_j}} - \frac{\partial \overline{u_i}}{\partial x_j} \overline{u_i' u_j'} - \overline{u_i' u_j' \frac{\partial u_i'}{\partial x_j}} - \frac{1}{\rho_0} \overline{u_i' \frac{\partial p'}{\partial x_i}} \\ & + \nu \overline{u_i} \overline{u_i' \frac{\partial^2 u_i'}{\partial x_j^2}} - 2 \epsilon_{ijk} \Omega_j \overline{u_i' u_k'} - \delta_{i3} \frac{g}{\rho_0} \overline{u_i' \rho'} \end{aligned} \quad (7)$$

The first and third terms on the right-hand-side are simplified by using the reverse product rule for differentiation and the incompressible form of the continuity equation. Then

$$\overline{u_i' u_j' \frac{\partial u_i'}{\partial x_j}} = \frac{1}{2} \frac{\partial}{\partial x_j} \left( \overline{u_i' u_i' u_j'} \right) \quad (8)$$

and

$$\overline{u_j u_i' \frac{\partial u_i'}{\partial x_j}} = \frac{1}{2} \frac{\partial}{\partial x_j} ( \overline{u_j u_i' u_i'} ) \quad (9)$$

The TKE equation for the system is

$$\begin{aligned} \frac{\partial \overline{u_i'^2}}{\partial t} = & - \frac{\partial}{\partial x_j} ( \overline{u_j u_i'^2} ) - 2 \overline{u_i' u_j'} \frac{\partial \overline{u_i}}{\partial x_j} - \frac{\partial}{\partial x_j} ( \overline{u_i'^2 u_j'} ) \\ & + \frac{2}{\rho_0} \overline{p' \frac{\partial u_i'}{\partial x_i}} - \frac{2}{\rho_0} \frac{\partial}{\partial x_i} ( \overline{u_i' p'} ) + \nu \overline{u_i' \frac{\partial^2 u_i'}{\partial x_j^2}} \\ & - 4 \epsilon_{ijk} \Omega_j \overline{u_i' u_k'} - 2 \delta_{i3} \frac{g}{\rho_0} \overline{u_i' \rho'} \end{aligned} \quad (10)$$

Changing notation so that  $[u_i] = [u, v, w]$ ,  $[x_i] = [x, y, z]$  and assuming horizontal homogeneity so that  $\frac{\partial}{\partial x} ( \overline{\quad} ) = \frac{\partial}{\partial y} ( \overline{\quad} ) = 0$  gives the component equations for turbulent kinetic energy:

$$\begin{aligned} \frac{\partial \overline{u'^2}}{\partial t} = & - 2 \overline{u' w'} \frac{\partial \overline{u}}{\partial z} - \frac{\partial}{\partial z} ( \overline{w' u'^2} ) + \frac{2}{\rho_0} \overline{p' \frac{\partial u}{\partial x}} \\ & - 4 \Omega_2 \overline{u' w'} + 4 \Omega_3 \overline{u' v'} \\ & + \nu ( \overline{u' \frac{\partial^2 u'}{\partial x^2}} + \overline{u' \frac{\partial^2 u'}{\partial y^2}} + \overline{u' \frac{\partial^2 u'}{\partial z^2}} ) \end{aligned} \quad (11)$$

$$\begin{aligned} \frac{\partial \overline{v'^2}}{\partial t} = & - 2 \overline{v' w'} \frac{\partial \overline{v}}{\partial z} - \frac{\partial}{\partial z} ( \overline{w' v'^2} ) + \frac{2}{\rho_0} \overline{p' \frac{\partial v}{\partial y}} - 4 \Omega_3 \overline{u' v'} \\ & + \nu ( \overline{v' \frac{\partial^2 v'}{\partial x^2}} + \overline{v' \frac{\partial^2 v'}{\partial y^2}} + \overline{v' \frac{\partial^2 v'}{\partial z^2}} ) \end{aligned} \quad (12)$$

$$\begin{aligned}
\frac{\partial \overline{w'^2}}{\partial t} = & - \frac{\partial}{\partial z} ( \overline{w'^3} ) - 2 \frac{1}{\rho_0} \frac{\partial}{\partial z} \overline{w' p'} + 2 \frac{1}{\rho_0} \overline{p' \frac{\partial w'}{\partial z}} - 2 \frac{g}{\rho_0} \overline{\rho' w'} \\
& + 4 \Omega_2 \overline{u' w'} + \nu ( \overline{w' \frac{\partial^2 w'}{\partial x^2}} + \overline{w' \frac{\partial^2 w'}{\partial y^2}} + \overline{w' \frac{\partial^2 w'}{\partial z^2}} )
\end{aligned} \quad (13)$$

where the terms on the right-hand-side are shear production, turbulent transport, pressure redistribution, pressure transport, buoyant production/damping, Coriolis redistribution, x-z rotational redistribution, and viscous dissipation; and the term on the left-hand-side is called the storage term.

## B. INTEGRATING FOR BULK TKE

Integrating over the depth of the mixed layer plus entrainment zone will give the bulk TKE for the layer. The storage term becomes

$$\int_{-h}^0 \frac{\partial \overline{u'^2}}{\partial t} dz = \frac{\partial h \langle \overline{u'^2} \rangle}{\partial t} \quad (14)$$

where  $\langle \rangle$  denotes the vertically integrated value. Turbulent transport and pressure transport terms integrate simply to zero, assuming no turbulent energy or pressure perturbations are transported across the boundaries. (Entrainment does not cross the interface at  $z = -h$ ; rather, it changes the depth of  $h$ .)

$$\int_{-h}^0 - \frac{\partial \overline{w' u'^2}}{\partial z} dz = \overline{w' u'^2} \Big|_0 - \overline{w' u'^2} \Big|_{-h} = 0 \quad (15)$$

$$\int_{-h}^0 - \frac{2}{\rho_0} \frac{\partial \overline{w' p'}}{\partial z} dz = \overline{w' p'} \Big|_0 - \overline{w' p'} \Big|_{-h} = 0 \quad (16)$$

Integration of the buoyant production/damping term and the x-z rotational redistribution term requires consideration of the approximately-linear flux profiles of temperature, salinity, and momentum within the layer, and the “jump condition” at the bottom of the layer. For any

conserved quantity  $C$ , the linear flux profile has a shape such as Figure (1) and the jump condition is

$$\overline{C' w'}|_{-h} = -w_e \Delta C \quad (17)$$

This introduces a new variable  $w_e$ , the entrainment velocity. In the absence of upwelling or downwelling,

$$\frac{\partial h}{\partial t} = w_e \quad (18)$$

Alternatively, if non-zero mean vertical velocity is included, then

$$\frac{\partial h}{\partial t} = w_e - \bar{w}|_{-h} \quad (19)$$

The temperature flux at the surface is

$$\overline{T' w'}|_0 = \frac{Q_0}{\rho_0 c_p} \quad (20)$$

where  $Q_0$  is the rate of cooling of the surface, and  $c_p$  is the specific heat of seawater at constant pressure. The surface salinity flux is

$$\overline{S' w'}|_0 = \bar{S} Vol \quad (21)$$

where  $Vol$  is the rate of addition or removal of water from the surface, the net result of precipitation, evaporation, melting, and freezing, expressed in units of length per time. The equations for the fluxes as functions of  $z$  then become

$$\overline{T' w'}(z) = \frac{Q_0}{\rho_0 c_p} \left(1 + \frac{z}{h}\right) - w_e \Delta T \left(\frac{-z}{h}\right) \quad (22)$$

and

$$\overline{S' w'}(z) = \bar{S} Vol \left(1 + \frac{z}{h}\right) - w_e \Delta S \left(\frac{-z}{h}\right) \quad (23)$$

Rather than treating the thermal expansion coefficient as a constant, it is allowed to vary linearly with depth.

$$\alpha(z) = a_0 - a_1 z \quad (24)$$



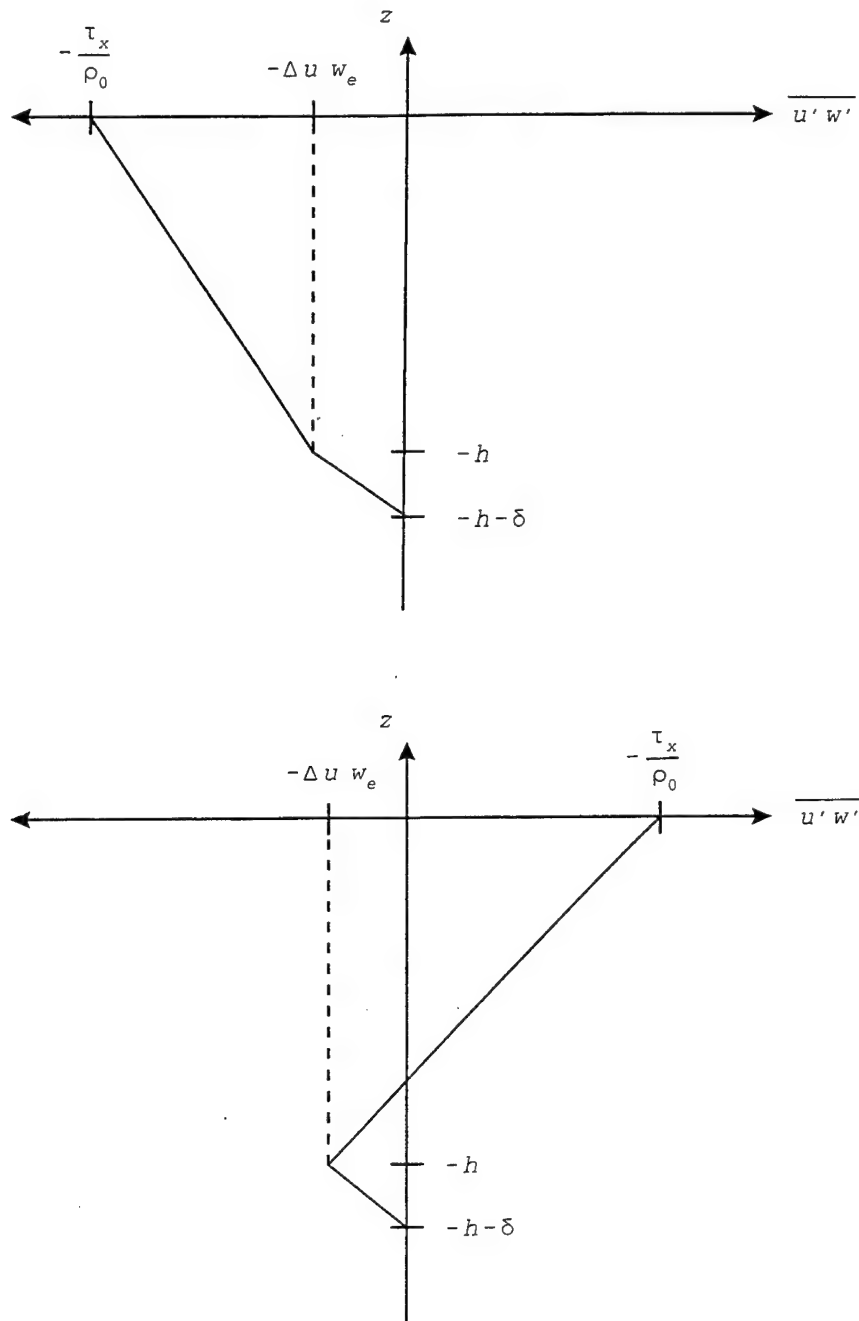


Figure 1. Flux profiles shown are for momentum, but would have similar shapes (piecewise linear) for any conserved quantity. The upper plot is for wind direction west to east, and the lower plot is for wind east to west.

Then the integration of the buoyant production and x-z rotational redistribution terms reduces to evaluating definite integrals of polynomials, so

$$\begin{aligned}
\int_{-h}^0 -2 \frac{g}{\rho_0} \overline{\rho' w'} dz &= 2 \int_{-h}^0 \overline{b' w'} dz \\
&= 2 \int_{-h}^0 \alpha(z) \overline{T' w'} dz - 2 \int_{-h}^0 \beta \overline{S' w'} dz \\
&= gh \left[ \frac{Q_0}{\rho c_p} \left( a_0 + \frac{a_1 h}{3} \right) + \beta \overline{S} Vol \right. \\
&\quad \left. - gh w_e \left[ \Delta T \left( a_0 + \frac{a_1 h}{1.5} \right) - \beta \Delta S \right] \right] \quad (25)
\end{aligned}$$

and

$$\int_{-h}^0 4 \Omega_2 \overline{u' w'} dz = 2 \Omega_2 h \left( \frac{\tau_x}{\rho_0} + w_e \Delta U \right) \quad (26)$$

By scaling, the second term on the right-hand-side of equation (26) is small and is neglected hereafter.

The integral of the shear production term has contributions only from the regions where there is velocity shear, near the surface and just below the bottom of the fully turbulent layer, as shown in Figure (2). Measurements have shown the velocity shear just below the surface to be proportional to the friction velocity, so that

$$\delta \overline{u} = m_3 u_* \sin \phi \quad (27)$$

where  $\phi$  is the angle from north clockwise to the wind vector,  $u_*^2 \equiv \frac{1}{\rho_0} \sqrt{\tau_x^2 + \tau_y^2}$ , and  $m_3$  is the constant of proportionality. The momentum fluxes at the surface and within the entrainment zone are approximated by the piecewise linear functions in Figure (1).

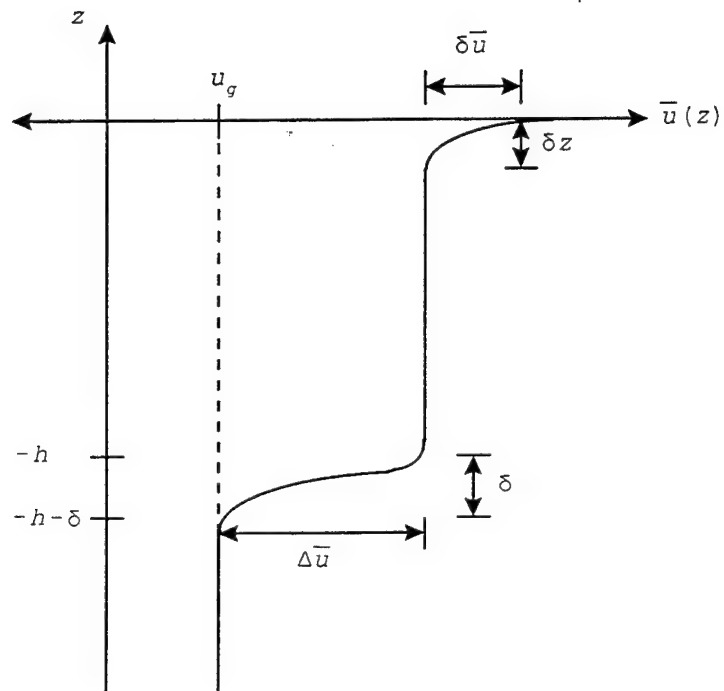


Figure 2. To model the production of turbulence by shear in the mean flow, values of vertical shear at the ocean's surface and in the entrainment zone are estimated rather than assumed infinite.

The surface momentum flux  $\overline{u'w'}|_0$  and the shear near the surface  $\frac{\partial \bar{u}}{\partial z}|_0$  are always opposite in sign, so that their product is always negative. Using the relationship

$$\frac{\tau_x}{\rho_0} = u_*^2 \sin \phi \quad (28)$$

the integral becomes

$$\begin{aligned} -2 \int_{-h-\delta}^0 \overline{u'w'} \frac{\partial \bar{u}}{\partial z} dz &= -2 \int_{-\delta z}^0 \overline{u'w'} \frac{\partial \bar{u}}{\partial z} dz - 2 \int_{-h-\delta}^{-h} \overline{u'w'} \frac{\partial \bar{u}}{\partial z} dz \\ &= -2 \overline{u'w'}|_0 \delta \bar{u} - 2 \overline{u'w'}|_{-h-\frac{\delta}{2}} \Delta \bar{u} \\ &= \frac{2m_3}{u_*} \left( \frac{\tau_x}{\rho_0} \right)^2 + w_e (\Delta \bar{u}) \end{aligned} \quad (29)$$

Considering the Coriolis redistribution, the Reynolds' stress is parameterized as proportional to the horizontal shear of the mean flow, which under horizontal homogeneity is zero. This means that because both forcing and response are the same everywhere, there can be no net transport of u turbulence in the v direction, and no net transport of v turbulence in the u direction.

$$4\Omega_3 \int_{-h}^0 \overline{u'v'} dz \propto \left( \frac{\partial \bar{u}}{\partial y} + \frac{\partial \bar{v}}{\partial x} \right) = 0 \quad (30)$$

Using the "return to isotropy" assumption of Rotta (1951), the pressure redistribution term becomes

$$\frac{2}{\rho_0} \int_{-h}^0 \overline{p' \frac{\partial u'}{\partial x}} dz = 2m_2 ( \langle E \rangle - 3 \langle \overline{u'^2} \rangle ) \langle E \rangle^{\frac{3}{2}} \quad (31)$$

where  $\langle E \rangle = ( \langle \overline{u'^2} \rangle + \langle \overline{v'^2} \rangle + \langle \overline{w'^2} \rangle )$  and  $m_2$  is a constant of proportionality.

Applying the product and chain rules for differentiation, the dissipation integral has terms of two forms,

$$\begin{aligned}
 & + \nu \int_{-h}^0 \left( \overline{u' \frac{\partial^2 u'}{\partial x^2}} + \overline{u' \frac{\partial^2 u'}{\partial y^2}} + \overline{u' \frac{\partial^2 u'}{\partial z^2}} \right) \\
 & = - \nu \int_{-h}^0 \left( \overline{\frac{\partial u'}{\partial x} \frac{\partial u'}{\partial x}} + \overline{\frac{\partial u'}{\partial y} \frac{\partial u'}{\partial y}} + \overline{\frac{\partial u'}{\partial z} \frac{\partial u'}{\partial z}} \right) dz \\
 & \quad + \nu \int_{-h}^0 \nabla^2 \left( \frac{\overline{u'^2}}{2} \right) dz
 \end{aligned} \tag{32}$$

The last term, viscous diffusion of turbulent energy, is negligible compared to both buoyant and shear production, or to turbulent transport. The remaining terms on the right-hand-side of equation (32) are u-component viscous diffusion and represent all of the dissipation of u TKE. Total dissipation is assumed to be a function of the net turbulent energy only, and is thus:

$$D = 2 m_1 \langle E \rangle^{\frac{3}{2}} \tag{33}$$

where  $m_1$  is a constant of proportionality and  $\langle \rangle$  denotes the mixed-layer average value. Since viscous dissipation occurs at the smallest scales, where kinetic energy is converted to heat, total dissipation is also assumed to be isotropic. The corresponding terms of each component equation would then be one third of the total dissipation.

Using the integral results of equations (14), (25), (26), (29), (31), and (33), the bulk equations for the components of turbulent kinetic energy are:

$$\begin{aligned}
\frac{\partial h \langle \overline{u'^2} \rangle}{\partial t} &= \frac{2m_3}{u_*} \left( \frac{\tau_x}{\rho_0} \right)^2 + w_e (\Delta \bar{u})^2 + 2\Omega_2 h \frac{\tau_x}{\rho_0} \\
&+ 2m_2 ( \langle E \rangle - 3 \langle \overline{u'^2} \rangle ) \langle E \rangle^{\frac{3}{2}} - \frac{2}{3} m_1 \langle E \rangle^{\frac{3}{2}}
\end{aligned} \tag{34}$$

$$\begin{aligned}
\frac{\partial h \langle \overline{v'^2} \rangle}{\partial t} &= \frac{2m_3}{u_*} \left( \frac{\tau_y}{\rho_0} \right)^2 + w_e (\Delta \bar{v})^2 \\
&+ 2m_2 ( \langle E \rangle - 3 \langle \overline{v'^2} \rangle ) \langle E \rangle^{\frac{3}{2}} - \frac{2}{3} m_1 \langle E \rangle^{\frac{3}{2}}
\end{aligned} \tag{35}$$

$$\begin{aligned}
\frac{\partial h \langle \overline{w'^2} \rangle}{\partial t} &= gh \left[ \frac{Q_0}{\rho c_p} \left( a_0 + \frac{a_1 h}{3} \right) + \beta \bar{S} Vol \right. \\
&- gh w_e \left[ \Delta T \left( a_0 + \frac{a_1 h}{1.5} \right) - \beta \Delta S \right] - 2\Omega_2 h \frac{\tau_x}{\rho_0} \\
&+ 2m_2 ( \langle E \rangle - 3 \langle \overline{w'^2} \rangle ) \langle E \rangle^{\frac{3}{2}} - \frac{2}{3} m_1 \langle E \rangle^{\frac{3}{2}}
\end{aligned} \tag{36}$$

### C. TEMPERATURE AND SALINITY EQUATIONS

Conservation principles, plus horizontal homogeneity, allow the potential temperature and salinity equations to be written as

$$\frac{\partial \bar{\theta}}{\partial t} = - \bar{w} \frac{\partial \bar{\theta}}{\partial z} - \frac{\partial \overline{\theta' w'}}{\partial z} \tag{37}$$

and

$$\frac{\partial \bar{S}}{\partial t} = - \bar{w} \frac{\partial \bar{S}}{\partial z} - \frac{\partial \overline{S' w'}}{\partial z} \tag{38}$$

Integrating over the mixed layer plus entrainment zone, and applying the jump condition, equation (17), the equations become

$$\frac{\partial \bar{\theta}}{\partial t} = \frac{1}{h} \left( \frac{Q_0}{\rho_0 c_p} - w_e \Delta \bar{\theta} \right) \quad (39)$$

and

$$\frac{\partial \bar{S}}{\partial t} = \frac{1}{h} \left( \bar{S} Vol - w_e \Delta \bar{S} \right) \quad (40)$$

#### D. BULK MOMENTUM EQUATIONS

Equation (1), after decomposing, averaging, making the Boussinesq approximation, assuming horizontal homogeneity, and neglecting viscous effects on the mean flow, gives the component equations for mean flow:

$$\frac{\partial \bar{u}}{\partial t} = - \bar{w} \frac{\partial \bar{u}}{\partial z} - \frac{1}{\rho_0} \frac{\partial \bar{p}}{\partial x} - 2\Omega_2 \bar{w} + 2\Omega_3 \bar{v} - \frac{\partial \overline{u'w'}}{\partial z} \quad (41)$$

$$\frac{\partial \bar{v}}{\partial t} = - \bar{w} \frac{\partial \bar{v}}{\partial z} - \frac{1}{\rho_0} \frac{\partial \bar{p}}{\partial y} - 2\Omega_3 \bar{u} - \frac{\partial \overline{v'w'}}{\partial z} \quad (42)$$

$$\frac{\partial \bar{w}}{\partial t} = - \bar{w} \frac{\partial \bar{w}}{\partial z} - \frac{1}{\rho_0} \frac{\partial \bar{p}}{\partial z} - g \left( \frac{\bar{\rho} - \rho_0}{\rho_0} \right) + 2\Omega_2 \bar{w} - \frac{\partial \overline{w'w'}}{\partial z} \quad (43)$$

The hydrostatic approximation is made, so that equation (43) becomes

$$\frac{\partial \bar{p}}{\partial z} = -\rho g \quad (44)$$

and upwelling is neglected here.

Although the  $\Omega_2$  terms were retained in the turbulence equations because  $w' \sim O(u')$ , they can be dropped here because  $\bar{w} \ll O(\bar{u}, \bar{v})$ . Also if the geostrophic and wind-driven flows are separated, equations (41) and (42) become

$$\frac{\partial \bar{u}}{\partial t} = - \bar{w} \frac{\partial \bar{u}}{\partial z} + 2\Omega_3 \bar{v} - \frac{\partial \overline{u'w'}}{\partial z} \quad (45)$$

and

$$\frac{\partial \bar{v}}{\partial t} = - \bar{w} \frac{\partial \bar{v}}{\partial z} - 2\Omega_3 \bar{u} - \frac{\partial \overline{v'w'}}{\partial z} \quad (46)$$

where  $\bar{u}$  and  $\bar{v}$  represent the wind-driven flow averaged over some short period of time.

Integrating equations (45) and (46) yields

$$\frac{\partial (h < \bar{u} >)}{\partial t} = 2\Omega_3 h < \bar{v} > + \frac{\tau_x}{\rho_0} \quad (47)$$

and

$$\frac{\partial (h < \bar{v} >)}{\partial t} = - 2\Omega_3 h < \bar{u} > + \frac{\tau_y}{\rho_0} \quad (48)$$

## E. ENTRAINMENT VELOCITY

Entrainment velocity must now be parameterized to close the system of equations; the local TKE budget at the bottom of the mixed layer, where the entrainment is occurring, can give a scale estimate. The sum of equations (11), (12), and (13) retains contributions to the storage term from shear production, turbulent transport, buoyant damping, and dissipation:

$$\begin{aligned} \frac{\partial (\overline{u'^2} + \overline{v'^2} + \overline{w'^2})}{\partial t} = & - 2 (\overline{u'w'} \frac{\partial \bar{u}}{\partial z} + \overline{v'w'} \frac{\partial \bar{v}}{\partial z}) \\ & - \frac{\partial}{\partial z} [ \overline{w' (E + 2 \frac{p'}{\rho_0})} ] \\ & - 2 \frac{g}{\rho_0} \overline{\rho' w'} - \epsilon \end{aligned} \quad (49)$$



where  $\epsilon = \nu \left( \overline{u' \frac{\partial^2 u'}{\partial x^2}} + \overline{u' \frac{\partial^2 u'}{\partial y^2}} + \overline{u' \frac{\partial^2 u'}{\partial z^2}} \right.$

$$\left. + \overline{v' \frac{\partial^2 v'}{\partial x^2}} + \overline{v' \frac{\partial^2 v'}{\partial y^2}} + \overline{v' \frac{\partial^2 v'}{\partial z^2}} \right.$$

$$\left. + \overline{w' \frac{\partial^2 w'}{\partial x^2}} + \overline{w' \frac{\partial^2 w'}{\partial y^2}} + \overline{w' \frac{\partial^2 w'}{\partial z^2}} \right) \quad (50)$$

Near  $z = -h$  both shear production and dissipation are small compared to the turbulence transported from above and to the amount being removed by buoyant flux, so that the balance is largely among storage, turbulent transport and buoyant damping.

$$\frac{\partial (\overline{u'^2} + \overline{v'^2} + \overline{w'^2})}{\partial t} \approx - \frac{\partial}{\partial z} \left[ \overline{w' (E + 2 \frac{P'}{\rho_0})} \right] - 2 \frac{g}{\rho_0} \overline{\rho' w'} \quad (51)$$

Each of these terms can be scaled on bulk variables, and the time scale for changes in turbulent energy at the bottom of the mixed layer can be thought of as the time required for a change in energy content to be turbulently diffused from the surface, which is posed here to depend upon  $h$  and  $\langle \overline{w'^2} \rangle$ .

$$\frac{\partial (\overline{u'^2} + \overline{v'^2} + \overline{w'^2})}{\partial t} \approx \frac{\langle \overline{E} \rangle w_e}{h} \quad (52)$$

$$- \frac{\partial}{\partial z} \left[ \overline{w' (E + 2 \frac{P'}{\rho_0})} \right] \approx \frac{m_4 \langle \overline{E} \rangle \sqrt{\langle \overline{w'^2} \rangle}}{h} \quad (53)$$

$$- 2 \frac{g}{\rho_0} \overline{\rho' w'} \approx - w_e g h (\alpha \Delta \overline{T} - \beta \Delta \overline{S}) \quad (54)$$

Combining and solving for entrainment velocity give

$$w_e = \frac{m_4 \langle \overline{E} \rangle \sqrt{\langle \overline{w'^2} \rangle}}{\langle \overline{E} \rangle + g h (\alpha \Delta \overline{T} - \beta \Delta \overline{S})} \quad (55)$$

## **F. NUMERICAL APPROACH**

The system of eight equations, summarized as Table (1), was cast as a MATLAB function, and the function was then called using the MATLAB utility ODE45, a Runge-Kutta ordinary differential equation solver that has automatic step-size control. The tolerance for the solver was relaxed from its default value of  $10^{-6}$  to  $10^{-4}$  for faster convergence.

$$\frac{\partial \bar{\theta}}{\partial t} = \frac{1}{h} \left( \frac{Q_0}{\rho_0 c_p} - w_e \Delta \bar{\theta} \right)$$

$$\frac{\partial \bar{S}}{\partial t} = \frac{1}{h} \left( \bar{S} Vol - w_e \Delta \bar{S} \right)$$

$$\begin{aligned} \frac{\partial (h \langle \bar{U} \rangle)}{\partial t} &= 2 \Omega_3 h \langle \bar{V} \rangle + \frac{\tau_x}{\rho_0} \\ \frac{\partial (h \langle \bar{V} \rangle)}{\partial t} &= -2 \Omega_3 h \langle \bar{U} \rangle + \frac{\tau_y}{\rho_0} \end{aligned}$$

$$w_e = \frac{m_4 \langle \bar{E} \rangle \sqrt{\langle \bar{w}^2 \rangle}}{\langle \bar{E} \rangle + gh [ (a_0 + a_1 h) \Delta \bar{T} - \beta \Delta \bar{S} ]}$$

$$\begin{aligned} \frac{\partial h \langle \bar{u}^2 \rangle}{\partial t} &= \frac{2m_3}{u_*} \left( \frac{\tau_x}{\rho_0} \right)^2 + w_e (\Delta \bar{u})^2 + 2 \Omega_2 h \frac{\tau_x}{\rho_0} \\ &\quad + 2m_2 ( \langle \bar{E} \rangle - 3 \langle \bar{u}^2 \rangle ) \langle \bar{E} \rangle^{\frac{3}{2}} - \frac{2}{3} m_1 \langle \bar{E} \rangle^{\frac{3}{2}} \end{aligned}$$

$$\begin{aligned} \frac{\partial h \langle \bar{v}^2 \rangle}{\partial t} &= \frac{2m_3}{u_*} \left( \frac{\tau_x}{\rho_0} \right)^2 + w_e (\Delta \bar{v})^2 \\ &\quad + 2m_2 ( \langle \bar{E} \rangle - 3 \langle \bar{v}^2 \rangle ) \langle \bar{E} \rangle^{\frac{3}{2}} - \frac{2}{3} m_1 \langle \bar{E} \rangle^{\frac{3}{2}} \end{aligned}$$

$$\begin{aligned} \frac{\partial h \langle \bar{w}^2 \rangle}{\partial t} &= gh \left[ \frac{Q_0}{\rho c_p} \left( a_0 + \frac{a_1 h}{3} \right) + \beta \bar{S} Vol \right. \\ &\quad \left. - gh w_e [ \Delta T \left( a_0 + \frac{a_1 h}{1.5} \right) - \beta \Delta S ] \right. \\ &\quad \left. - 2 \Omega_2 h \frac{\tau_x}{\rho_0} \right. \\ &\quad \left. + 2m_2 ( \langle \bar{E} \rangle - 3 \langle \bar{w}^2 \rangle ) \langle \bar{E} \rangle^{\frac{3}{2}} - \frac{2}{3} m_1 \langle \bar{E} \rangle^{\frac{3}{2}} \right] \end{aligned}$$

Table 1. Equations Used in the Model

## IV. OBSERVATIONAL DATA

### A. IMPORTANCE OF THE GREENLAND SEA REGION

As summarized by Visbeck et al. (1995), the Greenland Sea has long been considered to have characteristics favorable for deep water formation. Nansen, in 1906, observed only small differences in properties of Greenland Sea surface and deep waters, and proposed that deep water formation occurred there. Similar (but more modern) observations were made by Rudels et al. (1989), when mixing seemed to have recently extended to 1500 m. A synthesis of the physical explanations provided by Visbeck et al. (1995) and Schott et al. (1993) for how the region becomes favorable to deep convection includes the influences of the previous seasons as well as local forcing. Bourke et al. (1992) showed that during the ice-free months of the year, upper water conditions within the basin can be variable due largely to advection by the Jan Mayen Current. In early winter, as the marginal ice zone propagates rapidly eastward, brine release and entrainment act to increase the salinity of the surface waters, beginning to erode the buoyancy of the mixed layer. Deepening during this period may extend far enough into the warm Atlantic Intermediate Water, so that when subsequent cooling and stirring occur, warming by entrainment will dominate over surface cooling; the formation of ice is prevented and an ice-free area, surrounded on three sides by ice but open to the north, known as the Nordbukta, forms. The Nordbukta, situated over the Greenland Sea gyre, is then preconditioned for deep convection. Hence, the data discussed below, provided by Gascard and Lherminier (personal communication), were very well suited for use as a test case for the model.

## **B. OCEANOGRAPHIC DATA**

Two station soundings taken by the R/V Valdivia at 74.5 °N, 2.5° W, during February-March 1994 were examined. At this station, the ocean depth is more than 3600 m. For each sounding, the pressure, depth, in situ temperature, potential temperature, salinity, potential density referenced to the surface, potential density referenced to 2000 m, sound velocity, and dynamic height were available. In addition to the oceanographic data, each sounding had recorded the station number, date, hour, precise latitude and longitude, depth of sounding, sea surface temperature, sea surface salinity, wind speed and direction, and air temperature. Figure (3) shows February 16th's vertical profiles of potential temperature, salinity, and potential density referenced to the surface. A 200-m deep mixed layer of cold fresh water overlies more saline and warmer water; the buoyancy effects of temperature and salinity are in opposition, but salinity dominates. The 16 February profiles show that the magnitudes of the temperature and salinity gradients at the bottom of the mixed layer are very large, exceeding 0.1 C/m and 0.01 psu/m, respectively. Figure (4) shows profiles of the same quantities for March 19th, 31 days later; no intermediate soundings were available. The mixed layer is much deeper (600 m), and the entrainment of warmer more saline water has diminished the contrast between the two water masses; the buoyancy jump has been eroded by the mixed layer deepening.

Below 600 m the two soundings look very similar, especially if the March sounding is offset upward by about 30-40 m. This suggests a slow but steady downwelling speed of about 1 m/day, which is small compared to the average entrainment speed of about 13 m/day. Comparison of heat and salinity content between the two soundings gives an average loss of

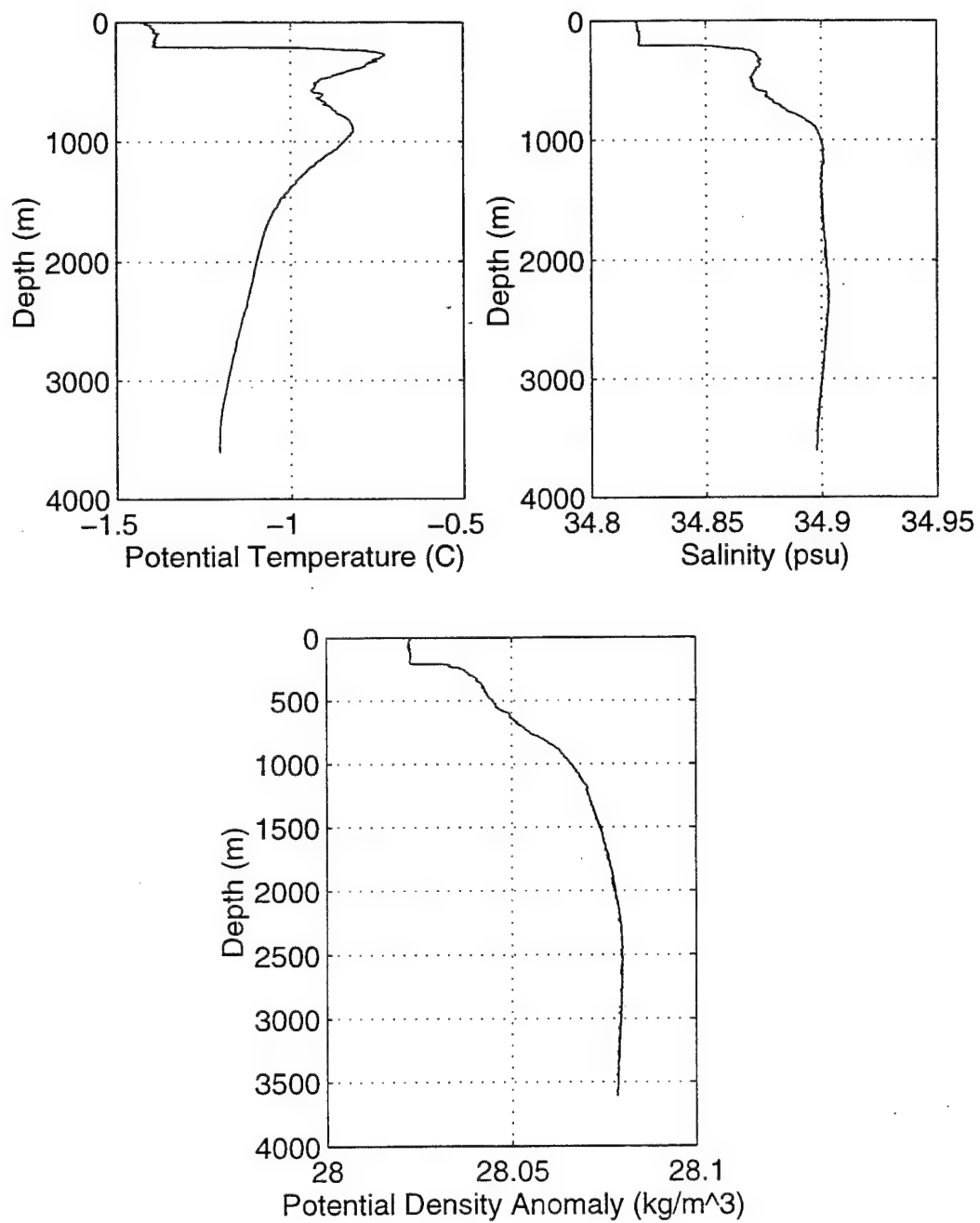


Figure 3. Sounding of 16 February 1994 shows a 200 m deep mixed layer overlying warmer, more saline water.

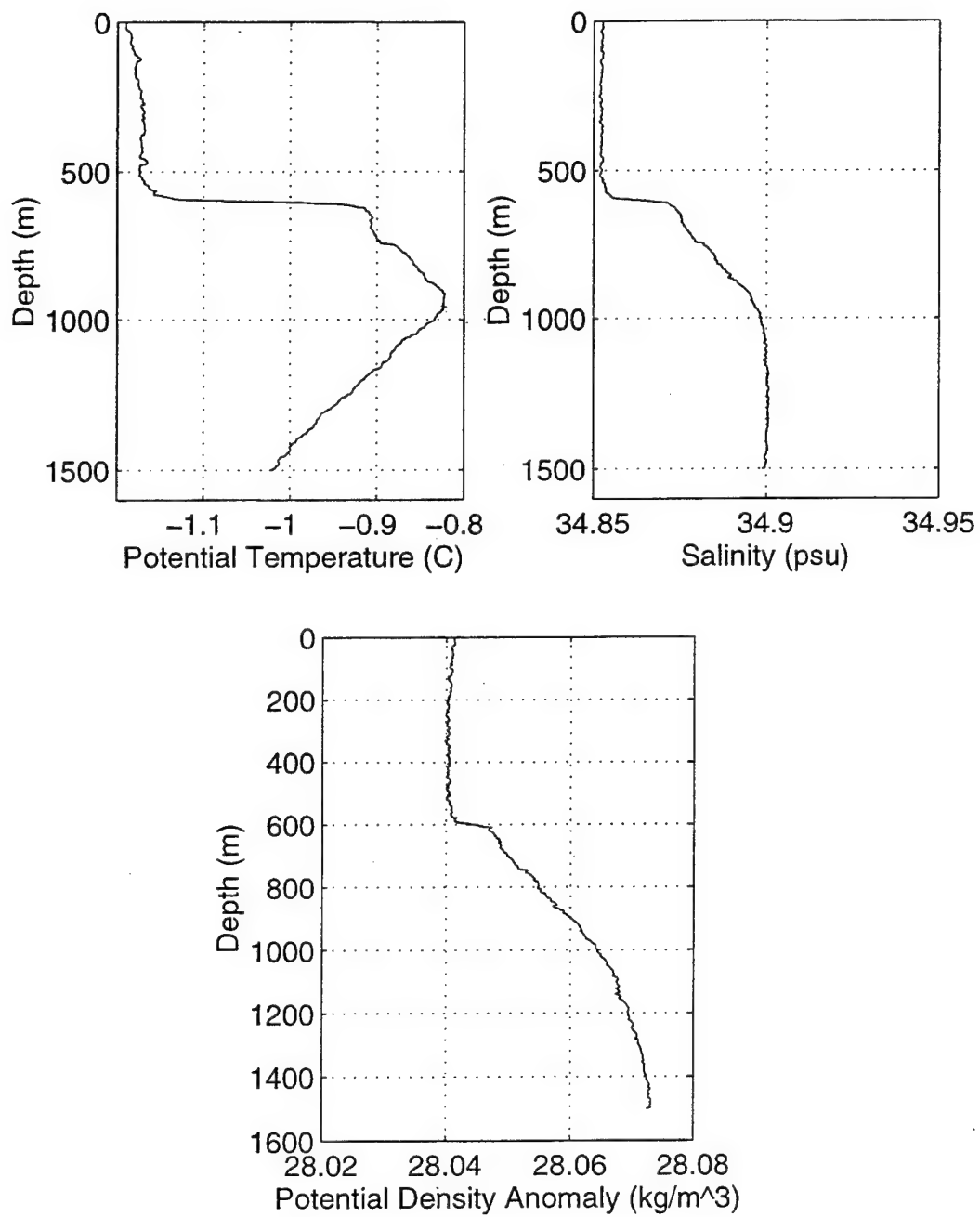


Figure 4. Sounding of 19 March 1994 shows mixed layer has deepened to 600 m.

130 W/m<sup>2</sup> and no surface flux in salinity. The similarity of profiles at depth as well as the apparent conservation of salinity gives some indication that horizontal advection is small, and that one-dimensional modeling should be useful for this case. As will be seen in Chapter V, the calculated Eckman transport for the layer suggests one-dimensional modeling as well.

### C. METEOROLOGICAL DATA

Meteorological data from the European Center for Medium Range Weather Forecasts (ECMWF) were available for February 2nd through May 31st. Parameters were six-hourly values of surface temperature, 2 m temperature, 10 m u-component of wind, 10 m v-component of wind, surface sensible heat flux, and surface latent heat flux. The values were interpolated from nearest-neighbor 2° grid points in the ECMWF analyses. Figure (5) shows the wind speed and associated wind stress for the period February 16th through March 19th, and Figure (6) shows the surface latent and sensible heat fluxes for the same period. The mean heat loss for the period indicated by these meteorological estimates is 182 W/m<sup>2</sup>, significantly larger than the actual average heat loss measured in the water column. This difference may be explained by lack of inclusion of net radiation or by error attributable to coarse resolution in the ECMWF product. Methods of correcting for this difference are discussed in Chapter V. Three events stand out as periods of large surface forcing, or storms; the latest of the three is the largest. It would be interesting to determine whether the mixed layer depth was relatively stable until this final large storm mixed the layer down to 600 m, or whether the deepening occurred gradually.



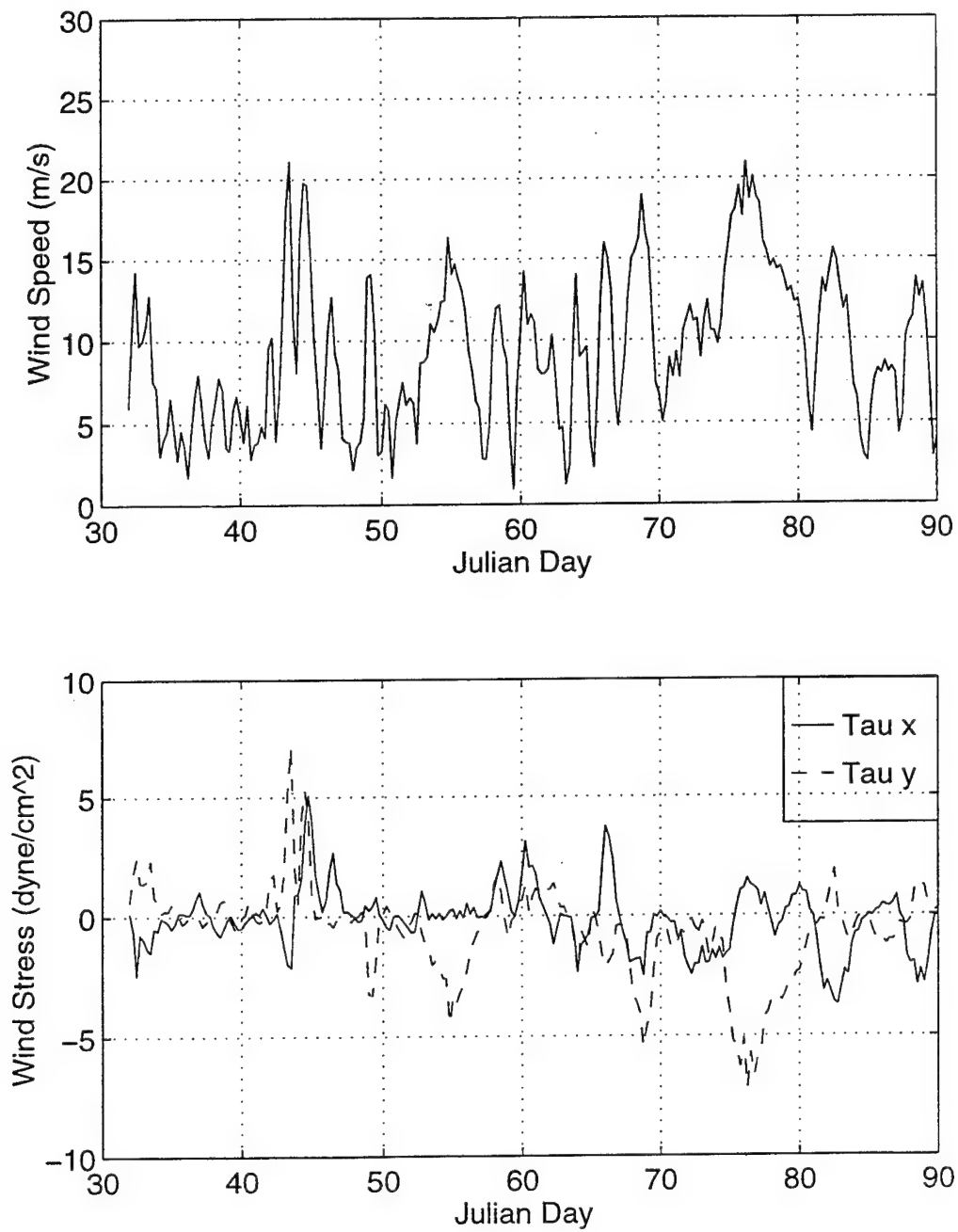


Figure 5. Meteorological data from ECMWF shows that wind speed and wind stress are highly variable over the period.

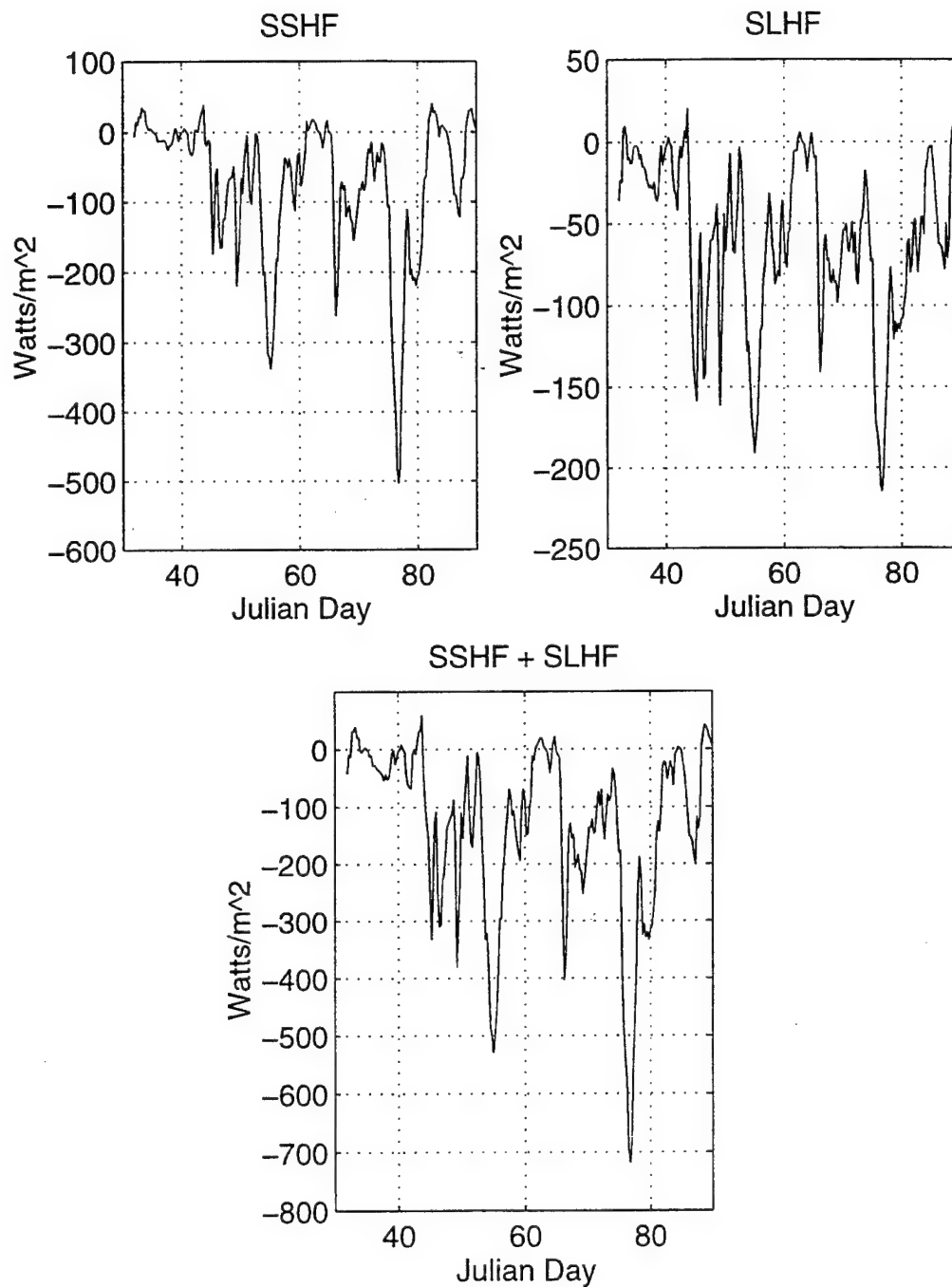


Figure 6. Three episodes of large surface heat loss stand out in the sum of surface sensible and latent heat fluxes, from ECMWF.



## V. MODEL RESULTS

### A. EFFECT OF THERMOBARICITY

The general behavior of the model was tested, comparing results in cases where thermobaricity is included to cases where it is neglected. These cases demonstrate that the increase in thermal expansion with pressure (depth) does increase the depth of mixing. Figures (7) and (8) show the deepening and the TKE components for a 25-day period with constant forcing of southerly winds ( $0.8217 \text{ dynes/cm}^2$  wind stress) and moderate cooling ( $100 \text{ W/m}^2$ ). Including the thermobaric effect increased deepening by 50%. Figures (9) and (10) show the deepening and the TKE components for a 25-day period with the same forcing except stronger cooling ( $400 \text{ W/m}^2$ ); including the thermobaric effect increased deepening by 33%. The point where the vertical turbulent energy exceeds the wind-driven turbulent energy (v-component in this case) can be interpreted as a shift from forced-convection dominant to free-convection dominant. The shift of regimes occurs earlier when thermobaricity is included.

Parcels above and below a typical Arctic region mixed-layer interface have a smaller buoyancy contrast with  $a_1 \neq 0$  than they have with thermobaricity neglected; they also have a smaller buoyancy contrast at depth than they would at shallower mixed layer depths. This diminished buoyancy jump will act to increase  $w_e$ , increasing the deepening rate. Further, the buoyancy flux at the bottom of the layer is proportional to both the entrainment velocity and the buoyancy jump; entrainment buoyancy flux is increased by both of these factors. Another process that deepens more due to thermobaricity is surface cooling; heat taken

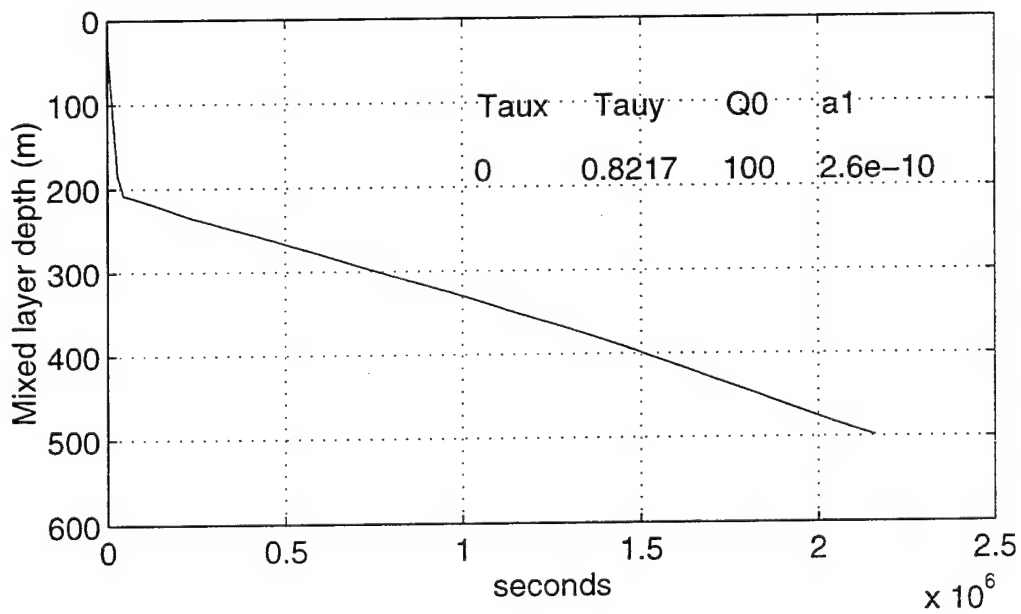
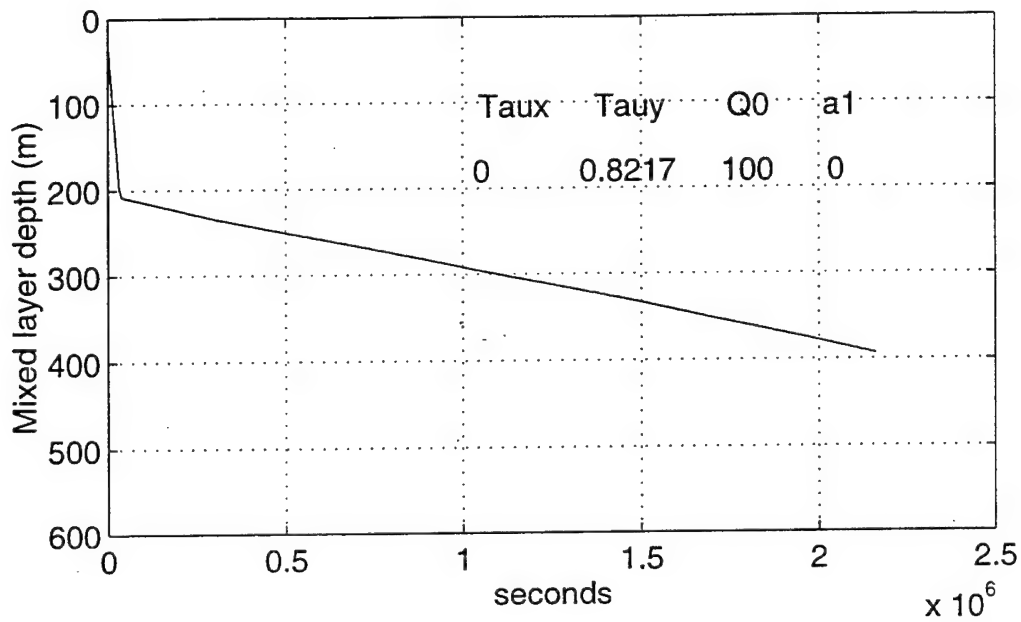


Figure 7. With  $100 \text{ W/m}^2$  of cooling, the model deepens the mixed layer 50% more when thermobaricity is included in the calculation ( $a_1 \neq 0$ ). Wind stresses Taux and Tauy are in  $\text{dynes/cm}^2$ ; heating Q0 is in  $\text{W/m}^2$ ; and  $a_1$  is in  $(\text{cm } ^\circ\text{C})^{-1}$ .

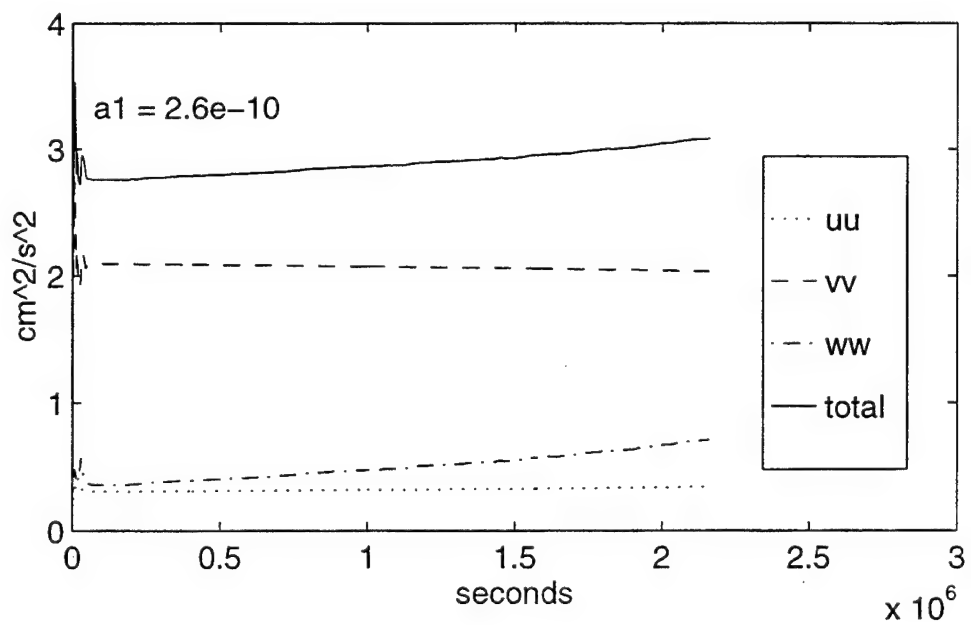
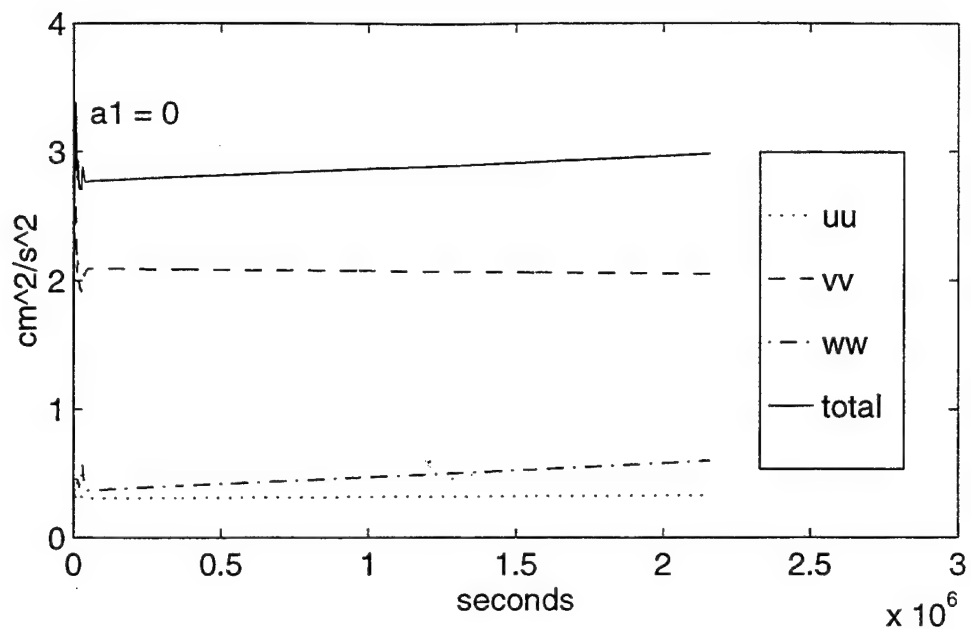


Figure 8. Velocity variances ( $\overline{u'^2}$ , for example) represent the turbulent energy present in the eddy field of each component. Comparison of the components in the plots above shows that the increase in deepening for the case with thermobaricity is due to increased turbulent energy in the vertical component.

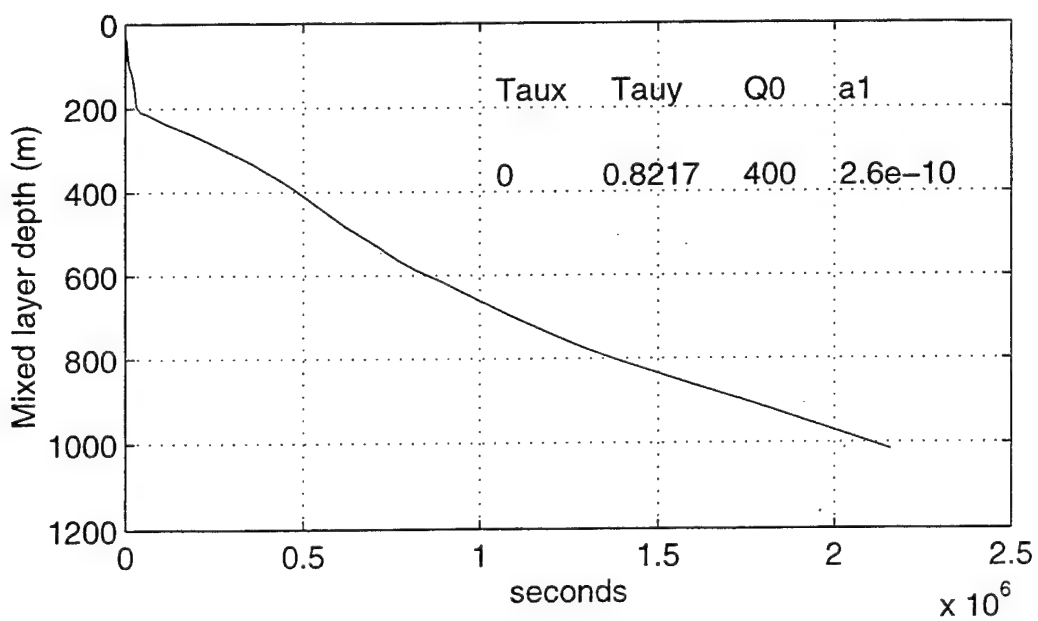
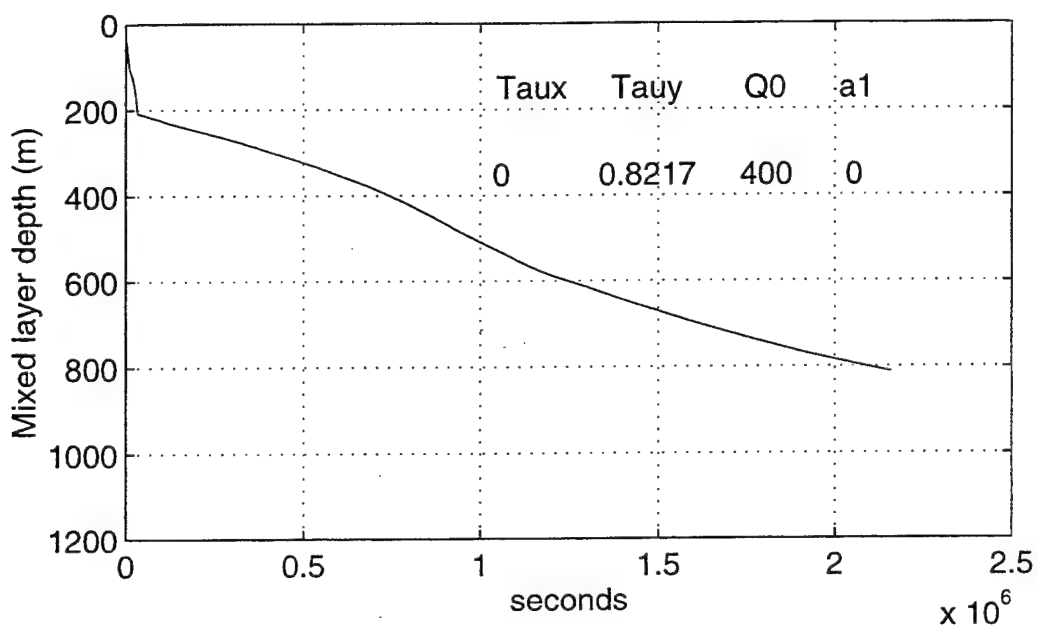


Figure 9. With 400 W/m<sup>2</sup> of cooling, the model deepens the mixed layer 33% more when thermobaricity is included in the calculation ( $a_1 \neq 0$ ). Wind stresses Taux and Ta<sub>xy</sub> are in dynes/cm<sup>2</sup>; heating Q0 is in W/m<sup>2</sup>; and a<sub>1</sub> is in (cm °C)<sup>-1</sup>.

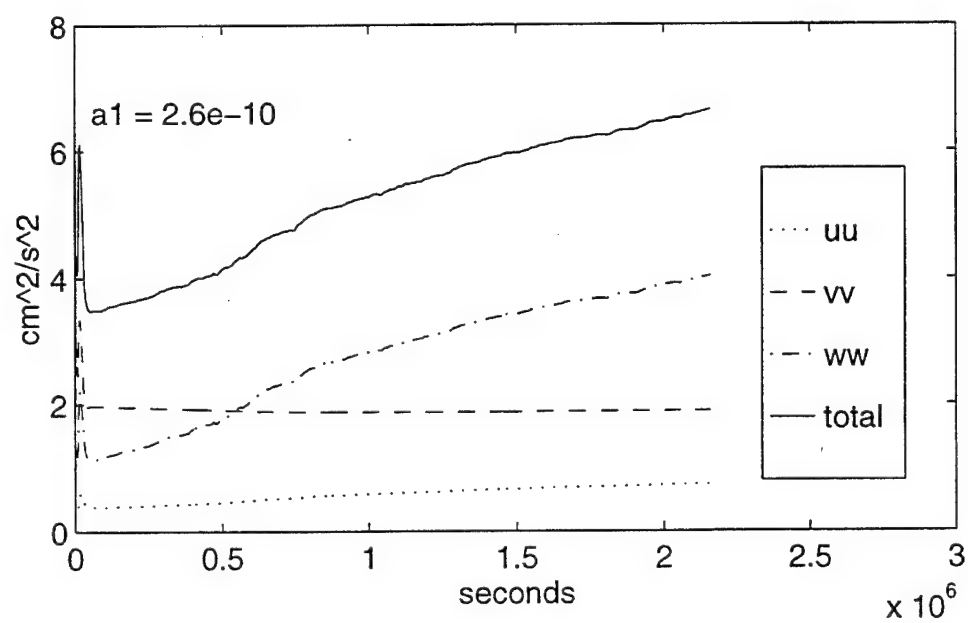
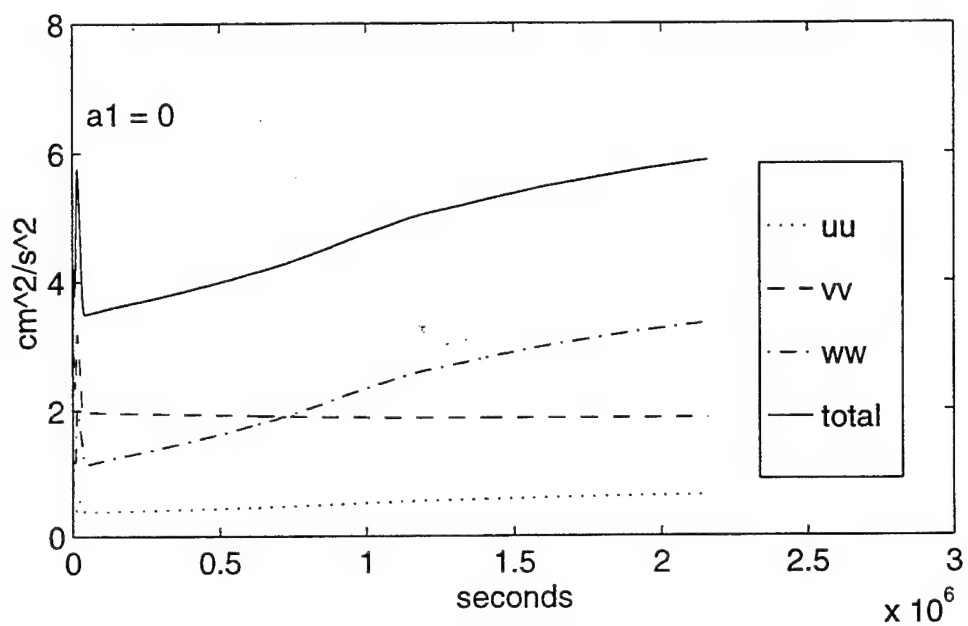


Figure 10. Turbulent energy components, represented by velocity variances, show that the increase in deepening is due to more vertical turbulent energy. The shift from forced convection to free convection occurs earlier with thermobaricity included.



out at the surface will have a greater density effect at depth than at shallower depths. Thermobaricity increased the deepening rate even for cases with as little as  $10 \text{ W/m}^2$  of cooling.

## **B. EFFECT OF COOLING**

To examine the sensitivity to seasonal cooling, the model was integrated for a period of 100 days from the initial profile of 16 February, using forcing corresponding to the means of u-wind and v-wind and two different rates of cooling. In the first case, the observed average heat loss of  $130 \text{ W/m}^2$  was used; in the second case, twice that. Figure (11) shows that doubling the rate of cooling has the effect of doubling the deepening rate; all other initial conditions and forcing are the same, and the heat is simply removed more quickly. Figure (12) shows that free convection dominates much sooner with the stronger cooling. It is also interesting to see the response of the horizontal turbulent energy components to the dramatic increase of vertical turbulent energy. They increase as a result of pressure redistribution; the turbulence is attempting to become more isotropic.

An interesting question is whether it was possible for the water column as measured on 16 February to be mixed to the bottom before summer ice melt and warming shut off deep mixing. Looking at Figure (11) again with this question in mind, it seems that there could not be enough time left even with very strong cooling for mixing to the bottom to have taken place in 1994.

## **C. EFFECT OF $\Omega_2$ ROTATION**

The direction of the wind has a potential effect on deepening because it can oppose or coincide with the direction of planetary rotation. To examine this effect, two 100-day

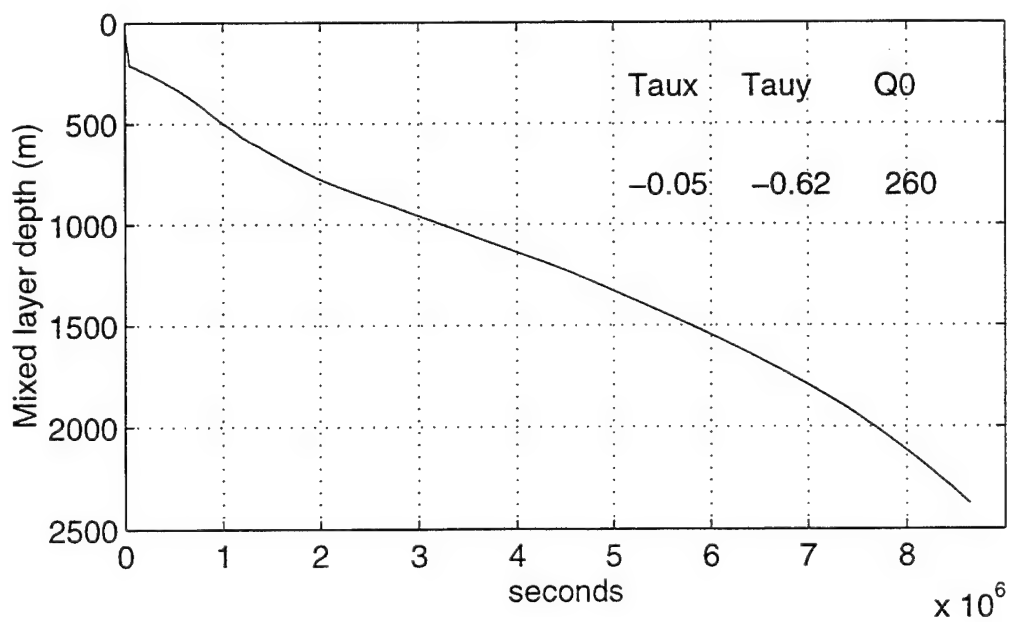
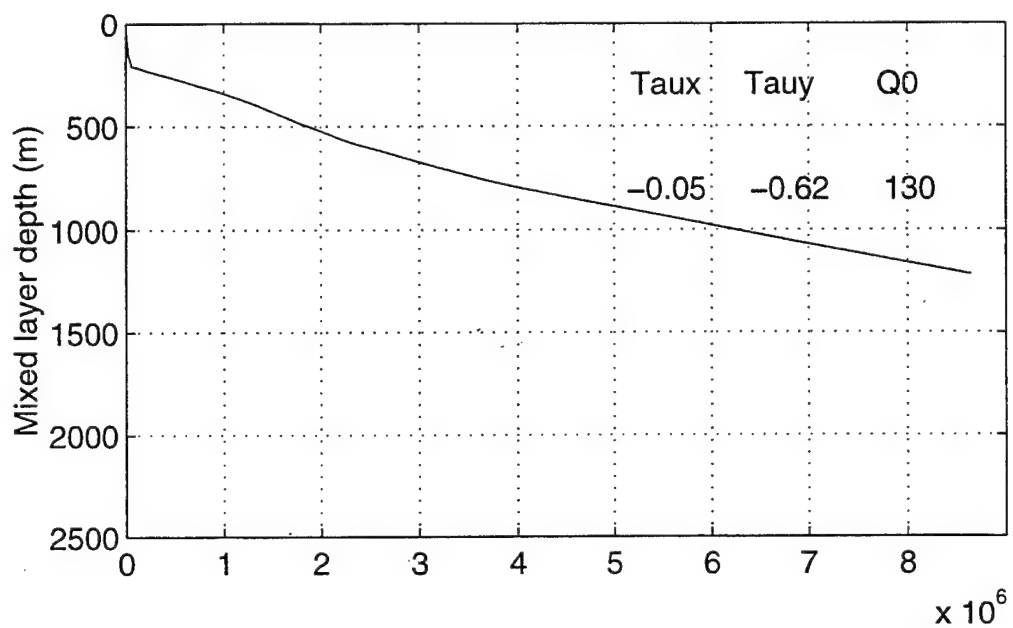


Figure 11. Doubling the cooling rate doubles the rate of deepening.

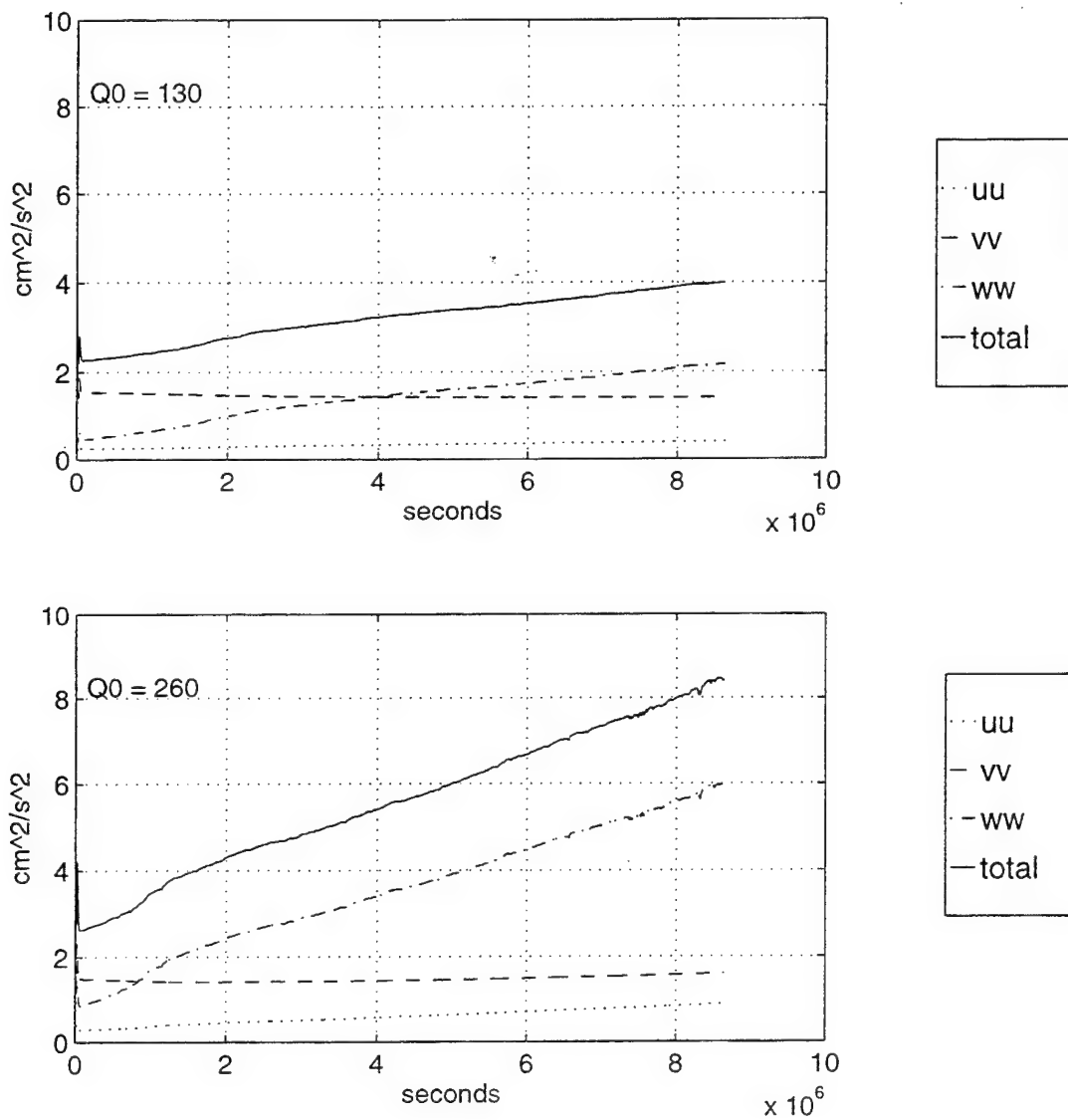


Figure 12. The vertical component of turbulent energy is dominant much sooner when cooling is  $260 \text{ W/m}^2$  vice  $130 \text{ W/m}^2$ .

cases were simulated, one with large westerly wind stress ( $+2 \text{ dynes/cm}^2$ ) and one with large easterly wind stress ( $-2 \text{ dynes/cm}^2$ ). Figure (13) shows that the westerly case deepened to 1289 m, while the easterly case deepened further, to 1468 m. In Figure (14), while the total turbulent energy for the two cases is about the same, the amount of energy that is in the vertical TKE is strikingly different. With easterly wind, u turbulent energy is converted to w turbulent energy (Figure (15) ); with westerly wind, w turbulent energy is diminished by conversion to u turbulent energy (Figure (16) ). The lower total energy for the deeper case is explained by the fact that there has been more buoyant damping (sometimes called buoyant consumption) associated with the increased entrainment.

#### **D. CONSTANT AVERAGE FORCING RESULTS COMPARED TO DATA**

When the model is integrated for 31 days with the mean wind components and observed average cooling, a mixed layer depth is calculated that is very close to that observed (627 m). However, averaging the vector wind components under-represents the amount of stirring; in order to make a more valid comparison, mean wind speed was computed and a typical wind direction chosen. Components of wind stress were then calculated from these, and the depth of mixing after integrating for 31 days was 733 m (Figure (17) ).

#### **E. TIME DEPENDENT FORCING**

The model was solved for the 31 days between the times of the CTD casts of 16 February and 19 March by linearly interpolating the winds and heat fluxes for times between the six hourly estimates from ECMWF. A final depth of 802 m was reached, and Figure (18) shows that the periods of more rapid deepening correspond to the more intense forcing events. The deepening of the mixed layer did not occur in one large surge during the third

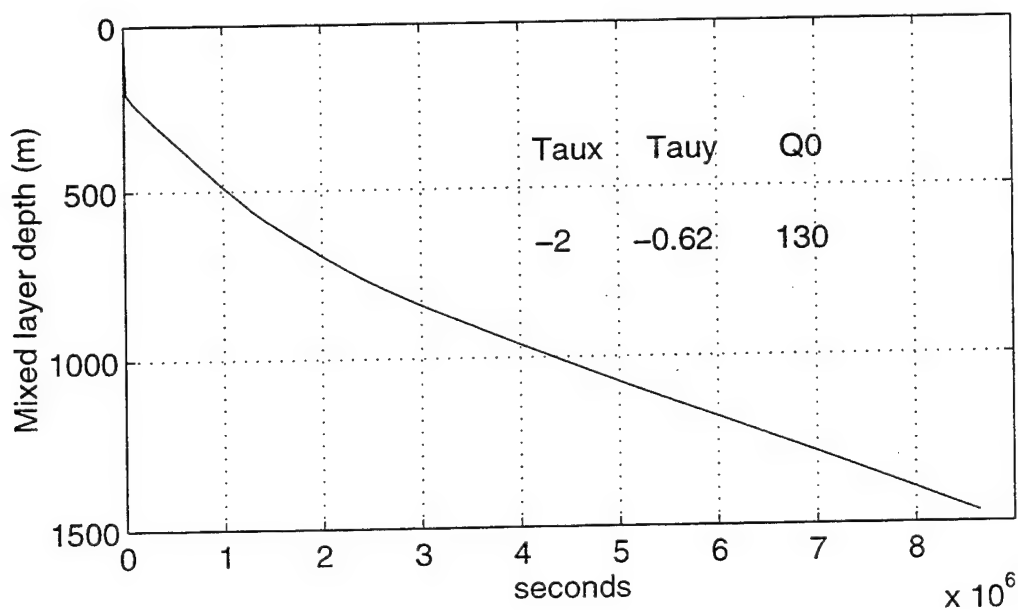
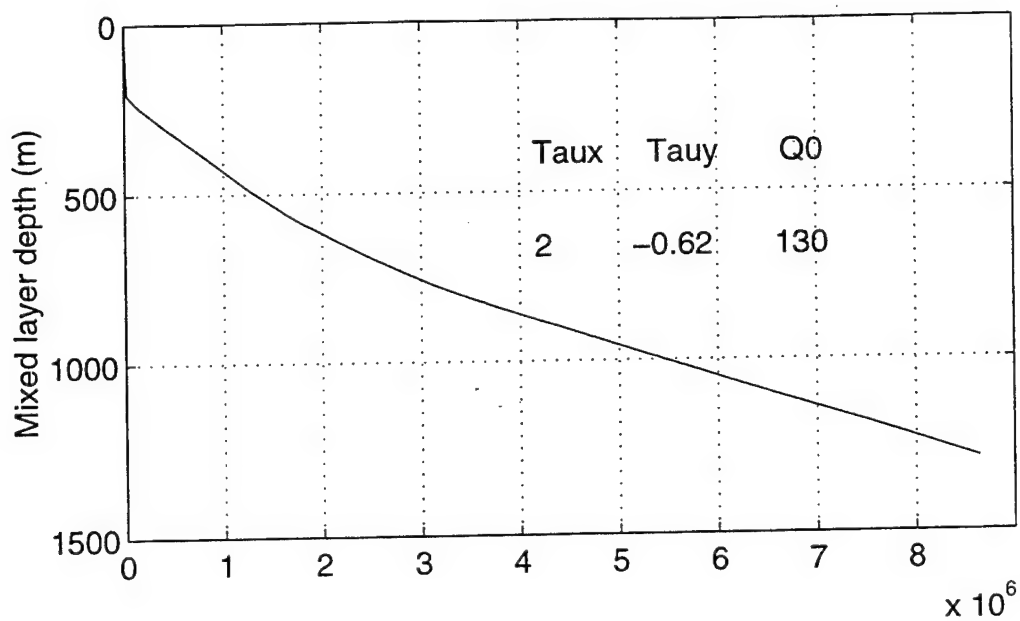


Figure 13. Westerly winds (from the west, upper plot) are not able to deepen the mixed layer as much as easterly winds (lower plot). Wind stress is in dynes/cm<sup>2</sup>; heating is in W/m<sup>2</sup>.

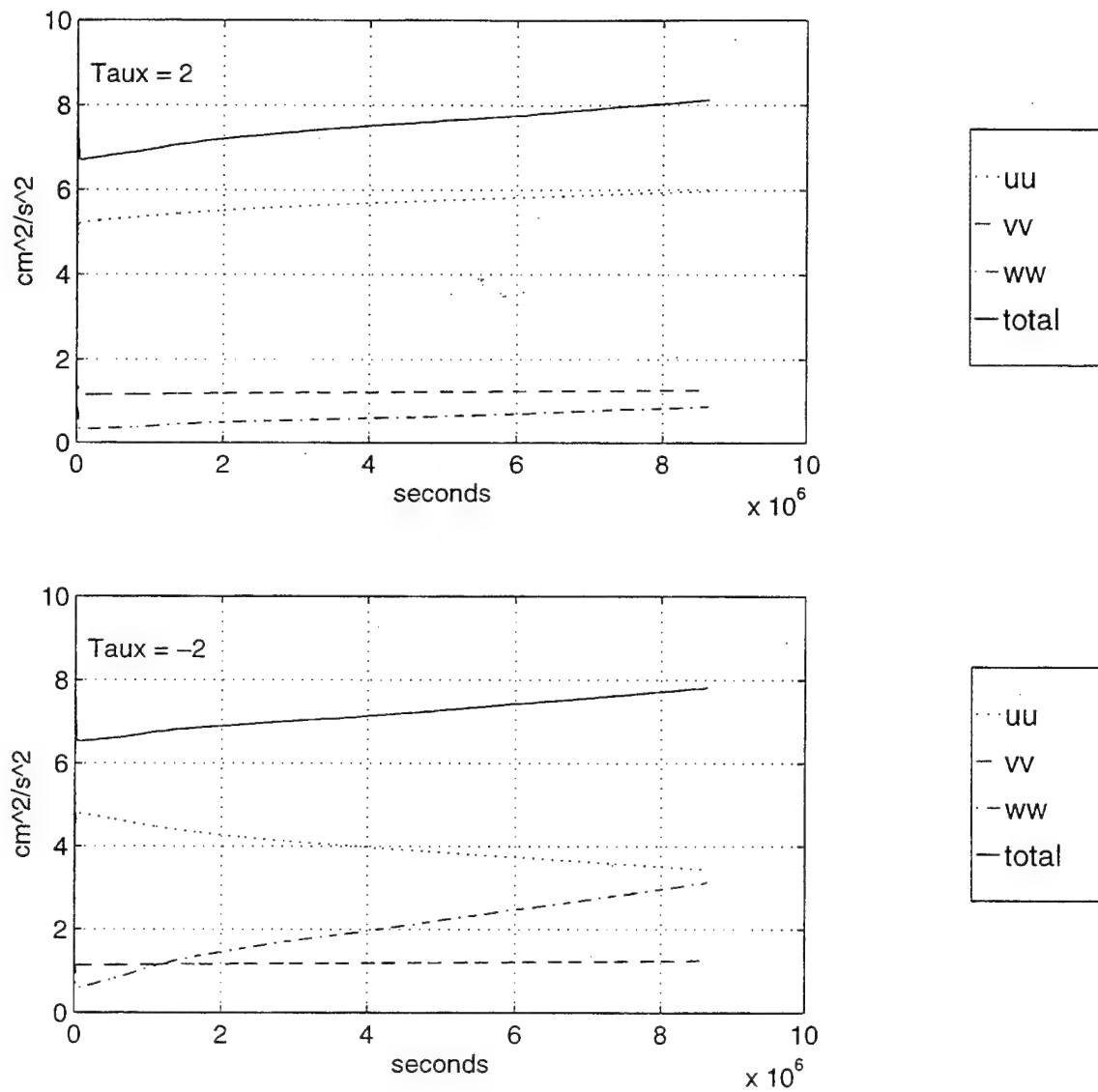


Figure 14. Total turbulent energy is nearly the same for the two cases, but the amount that is in the vertical eddies is different. Wind from the east (lower plot) puts more energy into the vertical component.

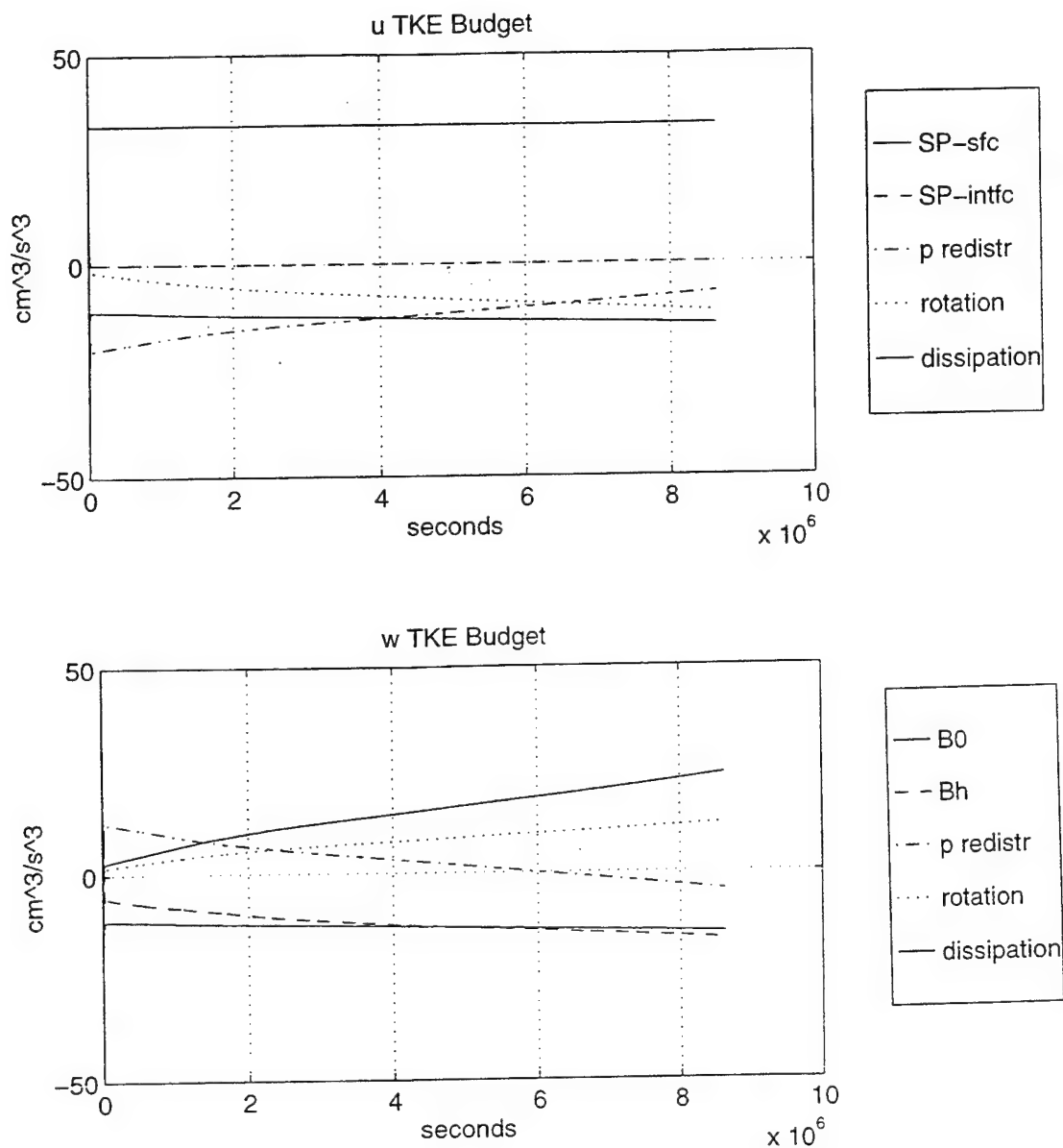


Figure 15. With forcing by easterly winds, the contribution from rotation is negative for u TKE and positive for w TKE: w receives energy from u.

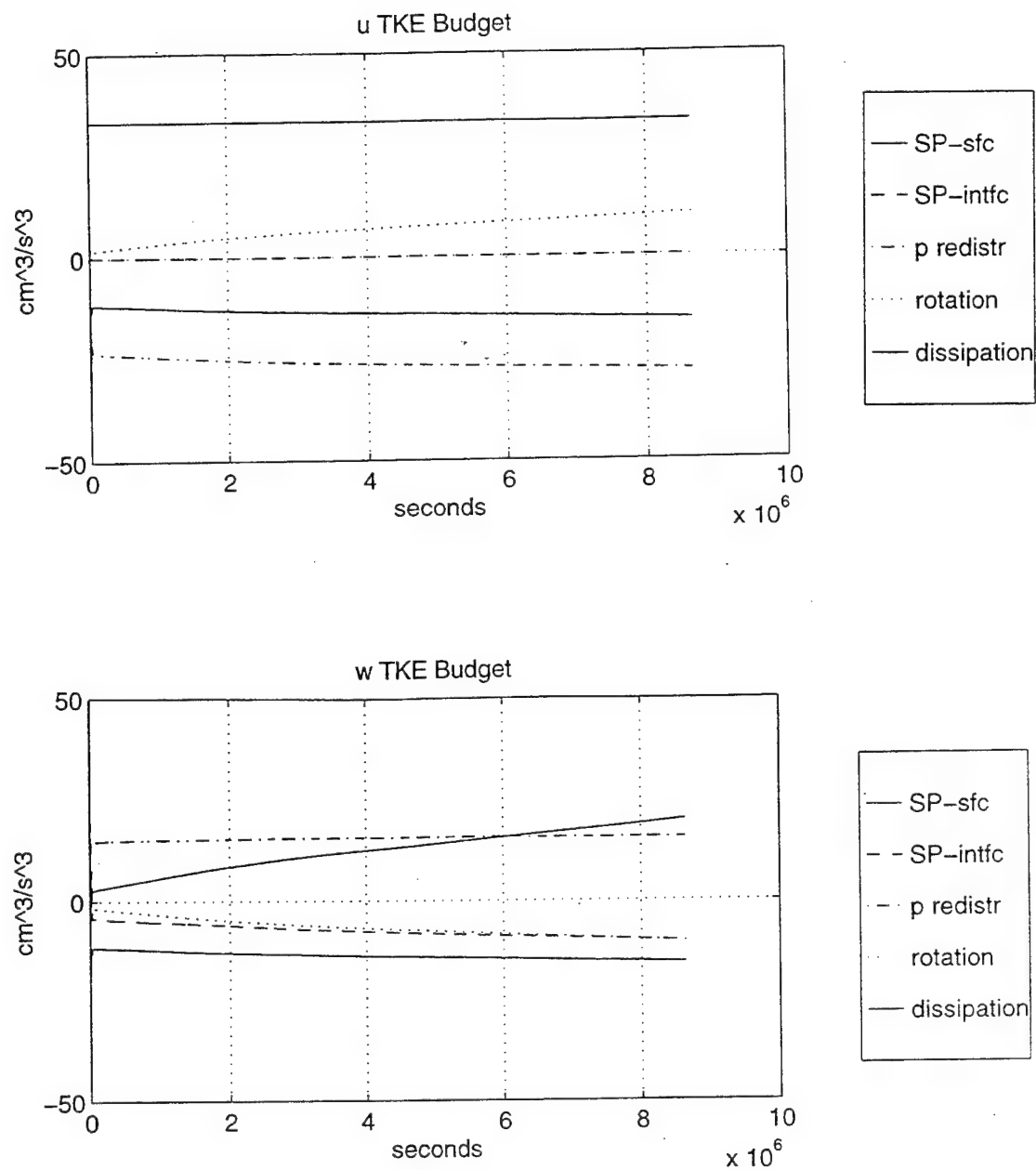


Figure 16. With forcing by westerly winds, the contribution from rotation is positive for u TKE and negative for w TKE: w gives up energy to u.



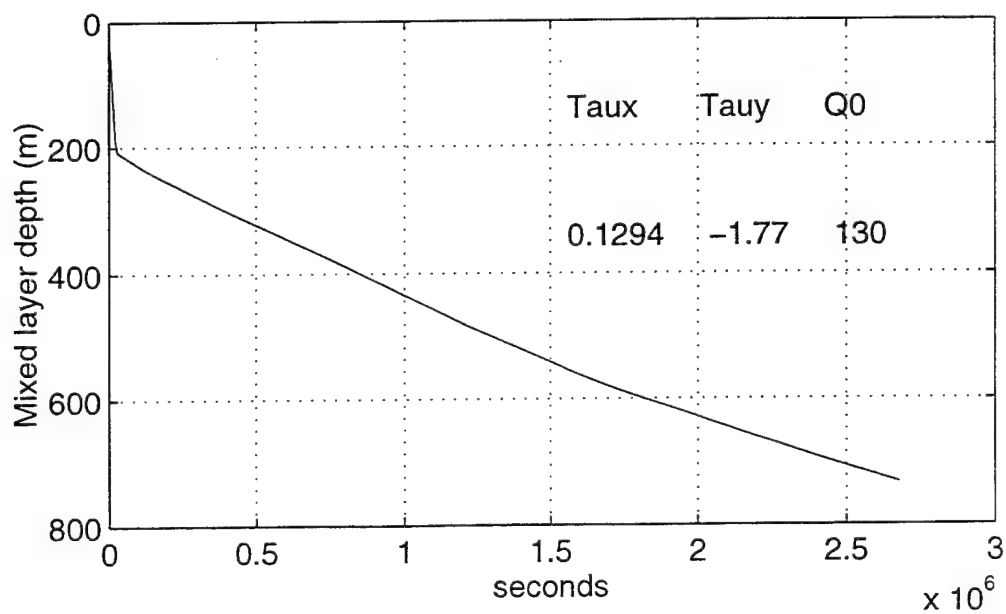
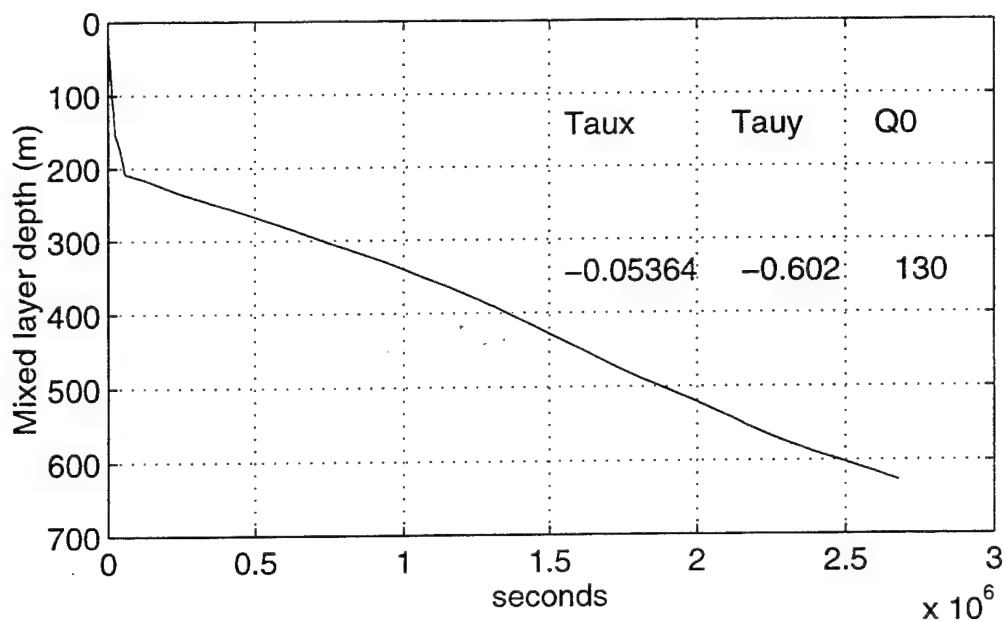


Figure 17. The upper plot shows deepening over 31 days with forcing computed from mean wind components. The lower plot shows deepening over 31 days with forcing computed from mean wind speed and a typical direction. Wind stress is in dynes/cm<sup>2</sup>; heating is in W/m<sup>2</sup>.

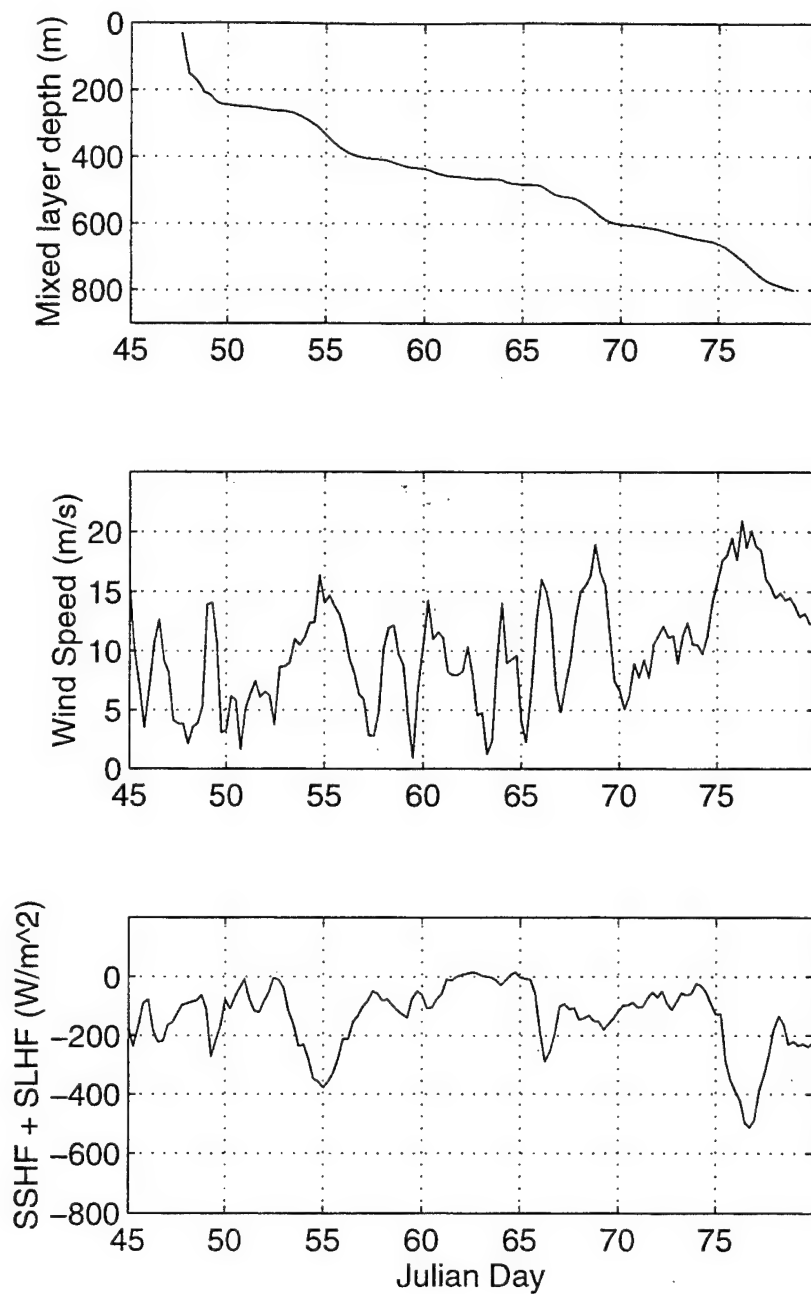


Figure 18. Mixed layer deepening is calculated with time-dependent forcing from meteorological data, and is plotted above graphs of wind speed and heat flux. The periods of more rapid deepening correspond to the periods of more intense forcing. In this model run the heat fluxes were corrected by scaling.

and strongest storm, but happened gradually. Even though the final forcing event was significantly larger than the other two, the layer was more resistant to deepening because it was already deeper. For a deeper layer, more energy is required for the same amount of entrainment simply because there is more water that must be kept turbulent.

Although the magnitude of heat removal from the ocean as indicated by the meteorological data was too high, there is a high degree of confidence in the qualitative correctness of that data; the storms' occurrences, their relative magnitudes, and the phase relationships of wind peaks to heat flux maxima are taken to be well represented. In other words, the shape of the surface heat flux time series should be retained even though its magnitude should be adjusted. Offsetting the heat flux by uniformly subtracting  $52 \text{ W/m}^2$  results in the correct total heat loss from the ocean, but results in periods of net warming of the ocean by the atmosphere in winter which are thought not to be realistic. Uniform scaling (multiplying by  $\frac{130}{182}$ ) did not present this disadvantage, and so was preferred. Another option of first adding  $50 \text{ W/m}^2$  as an approximate additional heat loss from the ocean due to net long wave radiation, then multiplying by  $\frac{130}{182+50}$ , was investigated later, but the results were so similar as to be almost indistinguishable.

Since momentum budgets were calculated in the model, they provided another check on the reasonableness of one-dimensional treatment of this problem. Integrating the mean wind-driven U and V of the mixed layer over each time interval, the mean wind-driven transport is computed. The progressive vector diagram for this transport is shown as Figure (19), and indicates the water column would move  $\sim 5 \text{ km}$  to the west, 90 degrees to the right of the mean wind direction, which is almost due south.

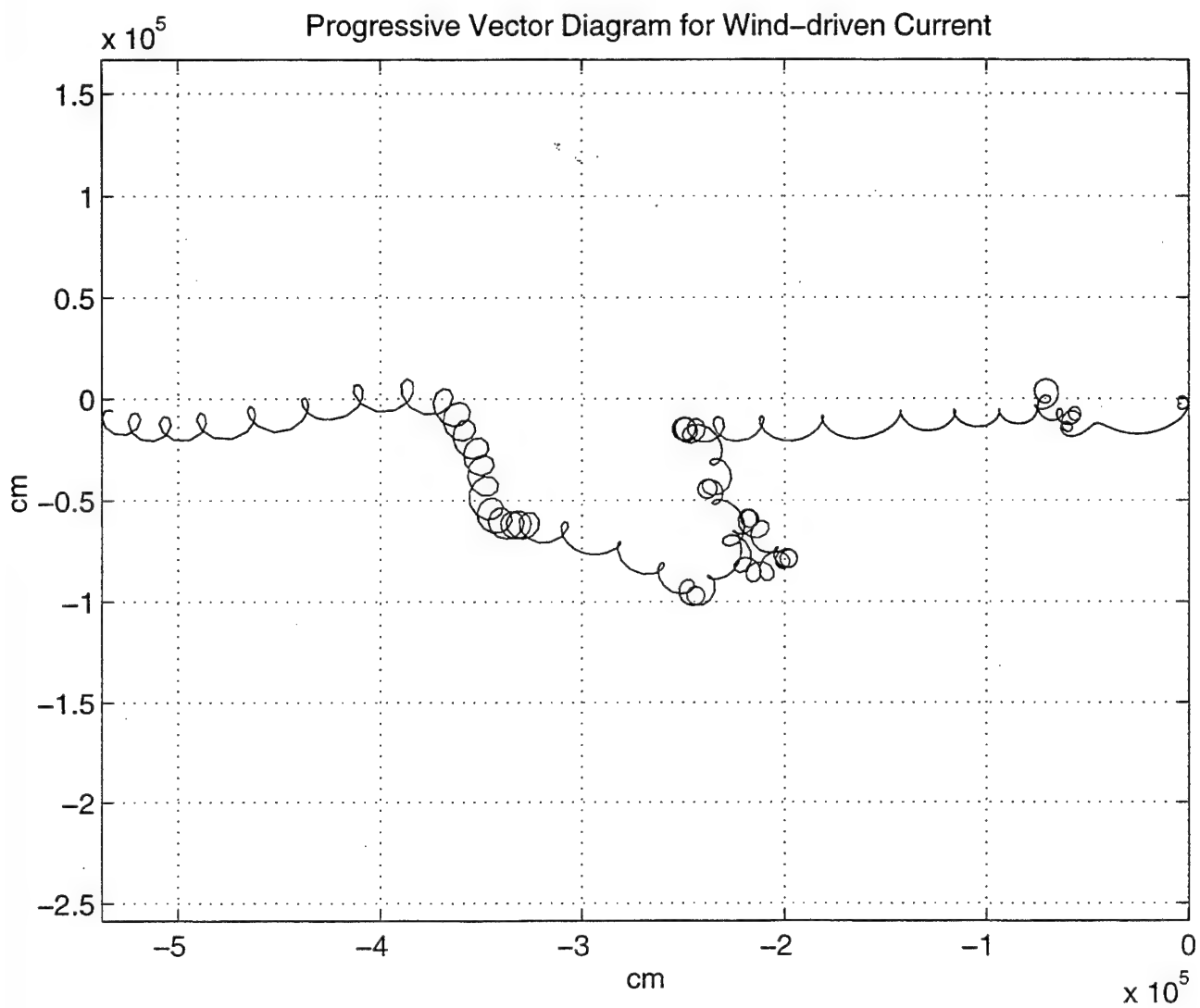


Figure 19. The time integral of the wind-driven velocities  $U$  and  $V$  of the mixed layer is plotted as a progressive vector diagram, showing the inertial effects and the mean transport of just over 5 km almost due west.

The components of turbulent kinetic energy are represented by  $\overline{u'^2}$ ,  $\overline{v'^2}$ , and  $\overline{w'^2}$ , and are plotted in Figure (20). What is striking in that figure is that v TKE was very dominant while w TKE accounted for only 10 to 20% of the total TKE during storm events: the turbulence was very anisotropic.

Figure (21) shows the contributing terms to u TKE. Shear production at the interface is always small, and pressure redistribution is the same order as shear production at the surface. Figures (22) and (23) are the corresponding plots for terms contributing to the v and w TKE budgets. In Figure (22), shear production at the surface is large, and v is losing even more energy through pressure redistribution than through dissipation. Figure (23) shows that the main source of vertical turbulent energy was pressure redistribution of wind energy. Also interesting is that the entrainment buoyancy flux is often as large as the surface buoyancy flux, and is plainly not a fixed fraction thereof.\* The integrated effect of rotation over the period is neutral, but rotation's effect during any particular storm may not be. Figure (24) is an enlargement of one section of the time series; the influence of rotation during the first event was to enhance entrainment, and during the second to inhibit entrainment. These observations show that for the same magnitude of forcing, a different depth of mixing may result. The phase relationship between wind stirring (via pressure redistribution) and surface buoyancy flux varies for different events as well. Could this also be a factor in the effectiveness of a particular storm for deep mixing?

---

\* A common approximation for entrainment by free convection in the atmospheric boundary layer is that the entrainment buoyancy flux is opposite in sign and a fixed fraction (order .2) of the surface buoyancy flux (Stull, 1988).

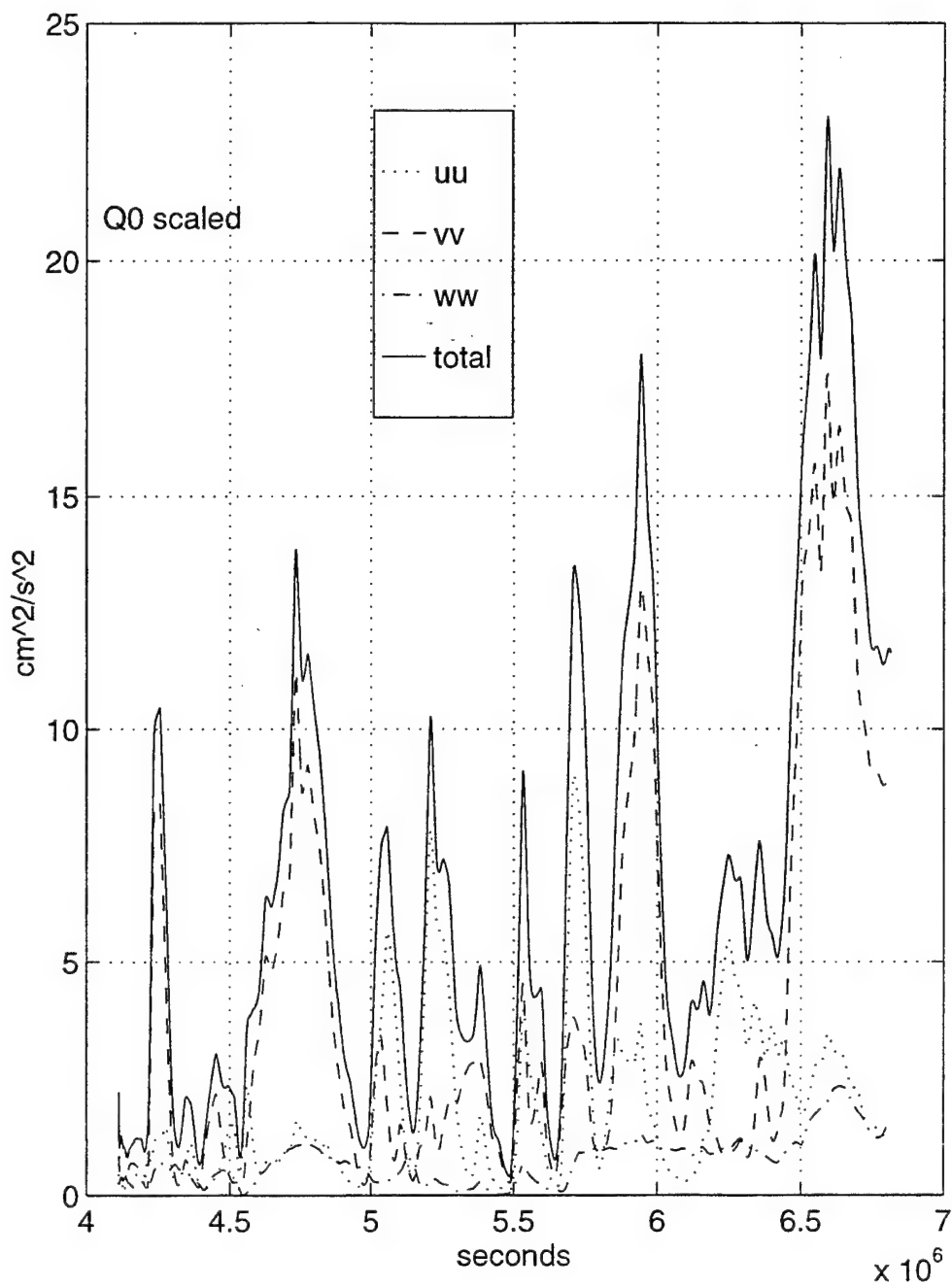


Figure 20. The turbulent kinetic energy components are plotted as functions of time for the time-dependent forcing case with surface heat flux scaled. Both wind stirring and cooling are vigorous, but  $v$  TKE dominates over  $w$  TKE.

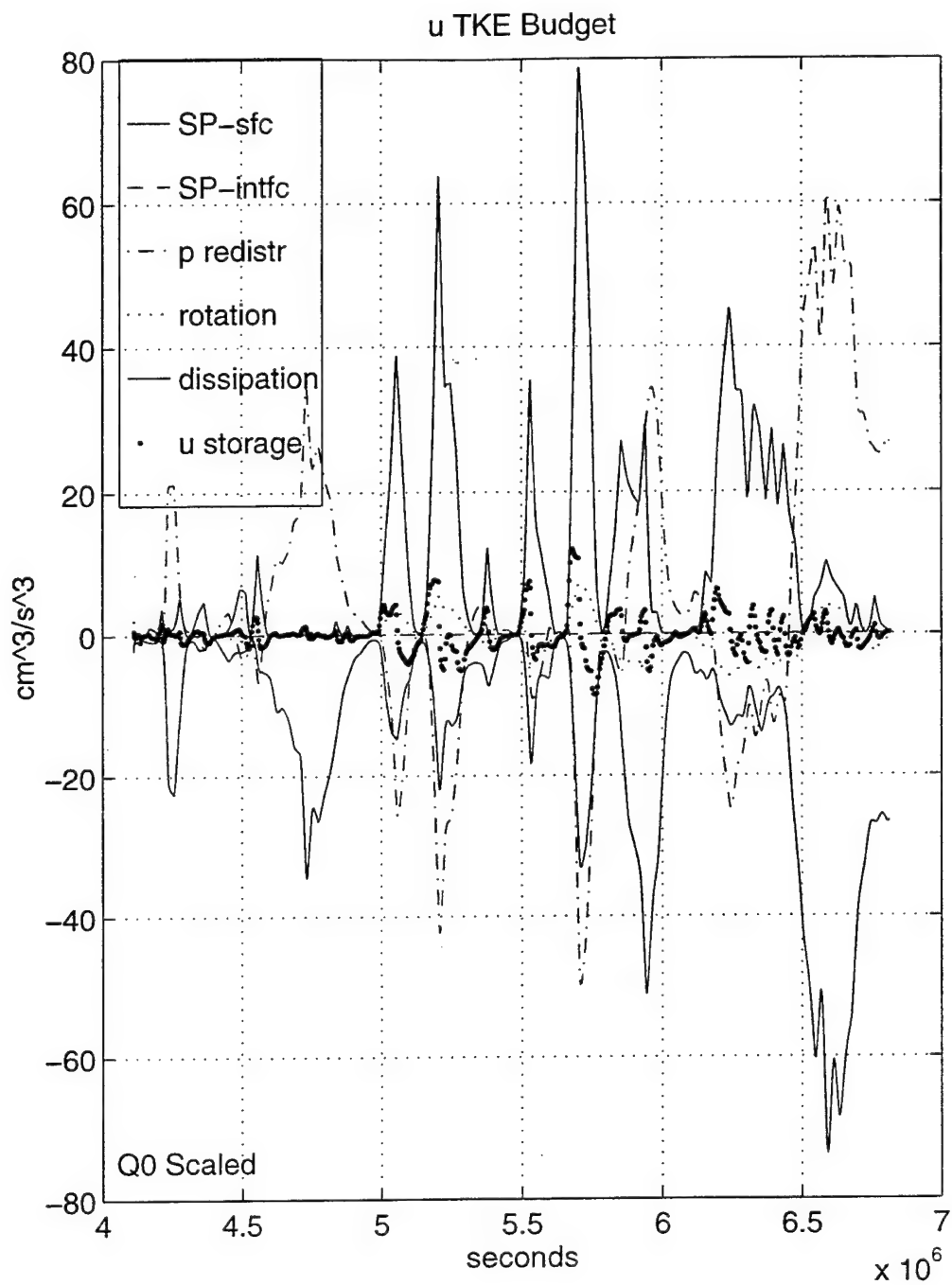


Figure 21. The contributions to u TKE are plotted as functions of time. They are: shear production at the surface, shear production at the interface, pressure redistribution, rotational redistribution, dissipation, and storage.

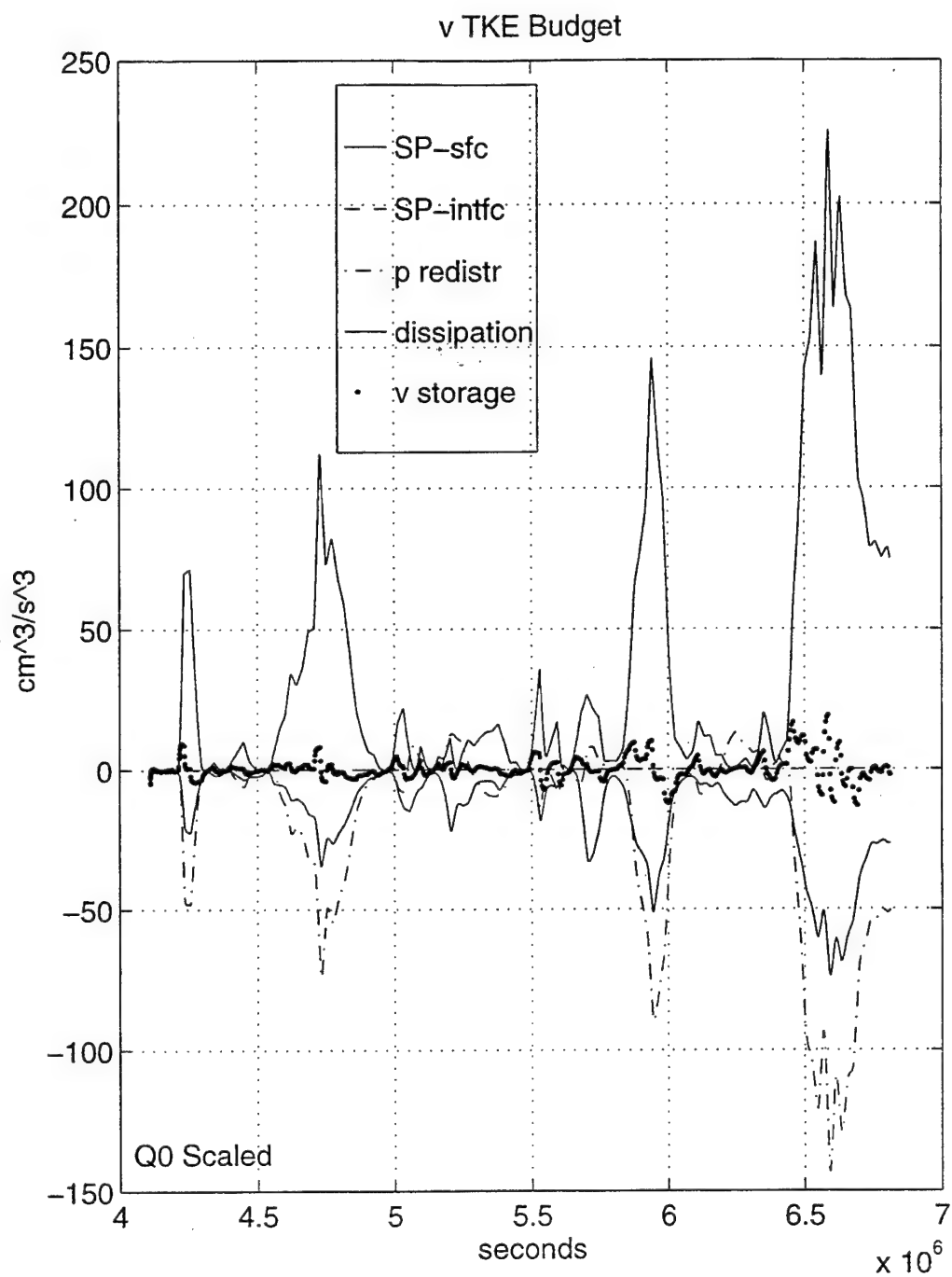


Figure 22. The contributions to v TKE are plotted as functions of time. They are: shear production at the surface, shear production at the interface, pressure redistribution, dissipation, and storage.



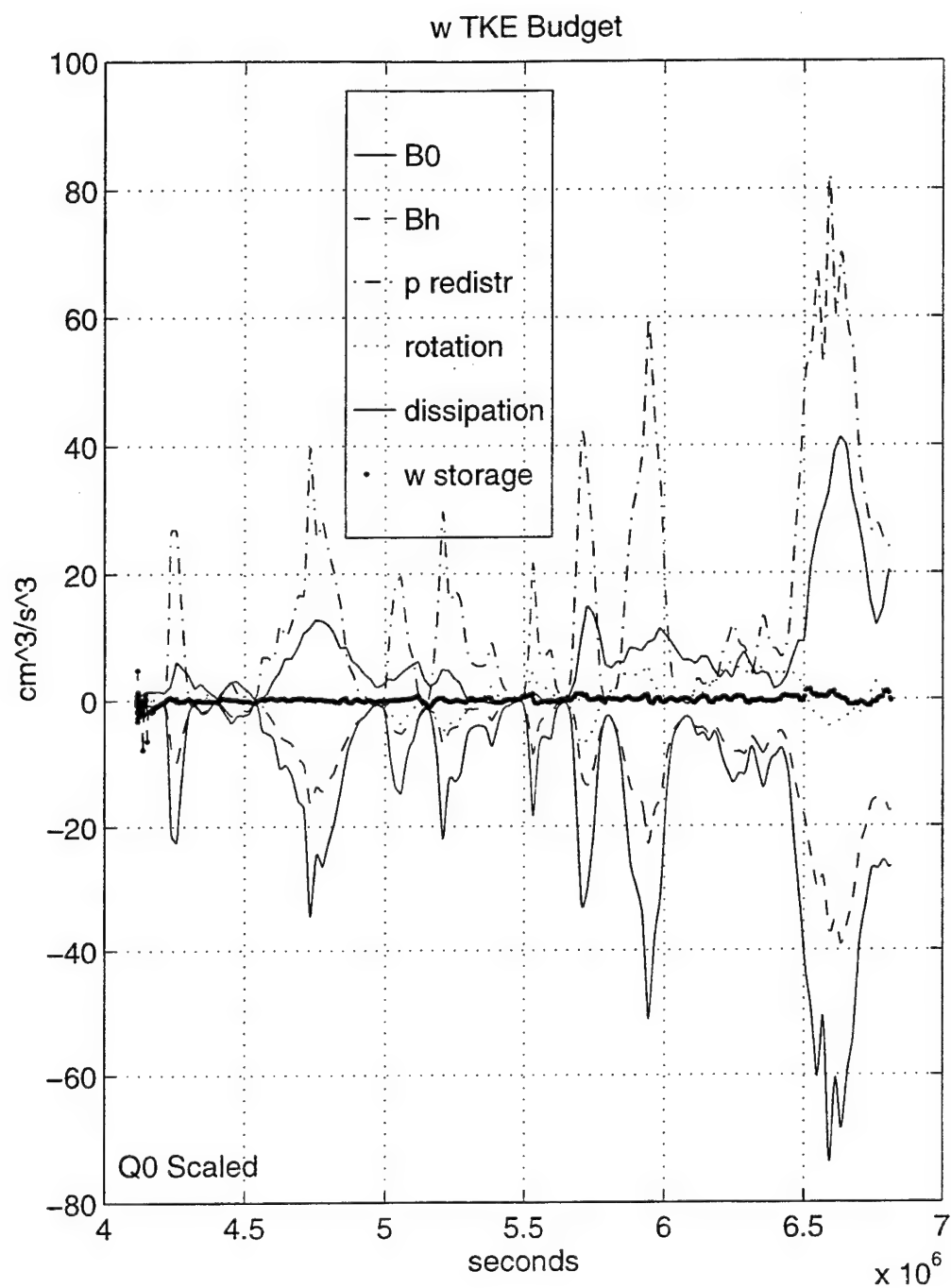


Figure 23. The contributions to w TKE are plotted as functions of time. They are: surface buoyancy flux, entrainment buoyancy flux, pressure redistribution, rotational redistribution, dissipation, and storage.

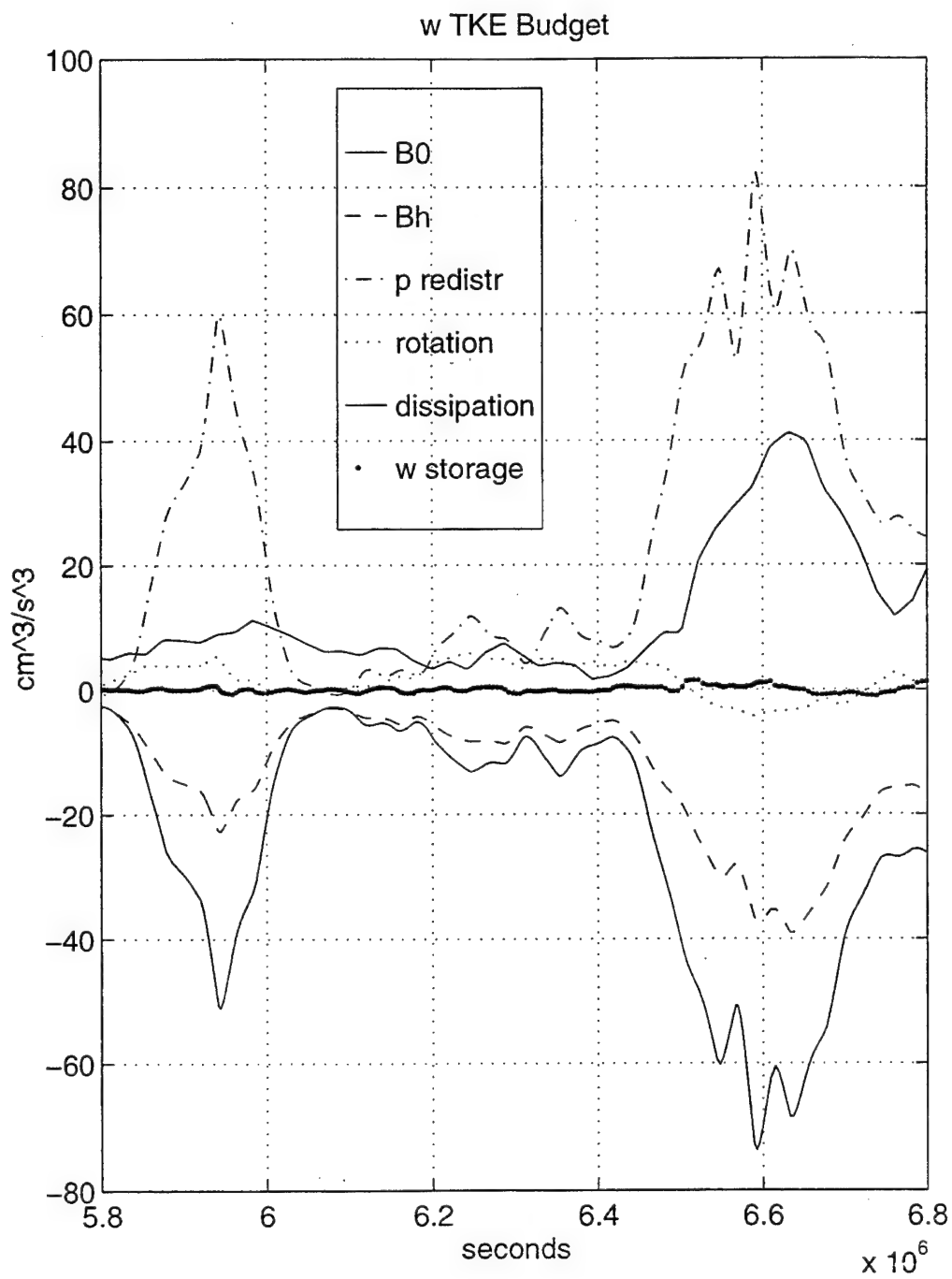


Figure 24. A section of Figure (23) is enlarged to show detail.

Figure (25) shows the various terms contributing to the total TKE of the mixed layer. The oscillatory behavior of the storage term is an interesting depiction of the mixed layer's ability to alternately store and then dissipate energy in response to wind surges.

Turning to the question of why the final mixed layer depth on 19 March is ~200 m too deep, two basic but related factors are felt to be responsible: the model does not retreat, and it may transport energy to the bottom of the layer too efficiently. After a period of low winds, when the wind stress suddenly increases, the ocean mixed layer requires time not only to re-stir the layer before entrainment recommences, but to transport energy surges downward before entrainment velocity can increase. Also, just after increased stirring, energy that is concentrated near the surface of the ocean gives more dissipation than the same amount of energy would if it were distributed more evenly throughout the layer. All of these effects can be corrected for by adjusting the model constants: the dissipation constant  $m_1$ , the pressure redistribution constant  $m_2$ , the shear production constant  $m_3$ , and the entrainment efficiency constant  $m_4$ . However, in this research, model constants were not adjusted to achieve quantitative agreement since such an adjustment would have meant tuning a very general model to match one specific observed case.

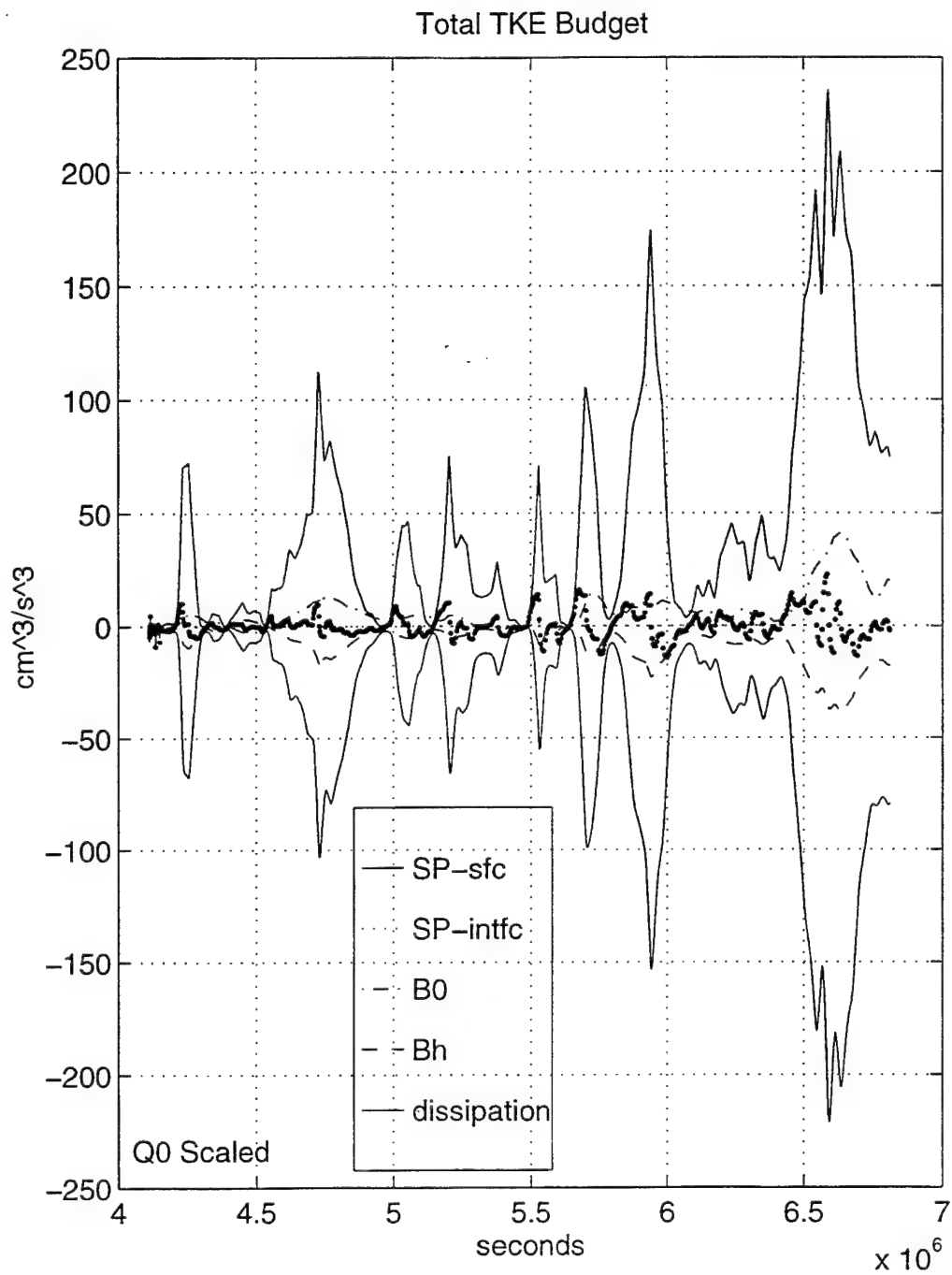


Figure 25. The contributions to total TKE are plotted as functions of time. They are: surface buoyancy flux, entrainment buoyancy flux, surface shear production, dissipation, and storage.



## VII. CONCLUSIONS

### A. SUMMARY

Coupling of the ocean to the atmosphere through deep mixed layers in polar regions is fundamental to our climate system, and much of the energy exchange occurs episodically during storms. In order to understand the physics of the ocean mixed layer response to storms, a bulk turbulence-closure mixed layer model was developed and was used to simulate an observed case of deep polar sea mixing.

The model included budgets for potential temperature, salinity, horizontal momentum, and unsteady three-component turbulent kinetic energy. In addition to shear production, surface buoyancy flux, entrainment buoyancy flux, pressure redistribution, and dissipation, realistic treatment was also given to thermobaric enhancement of buoyancy flux and to Coriolis' effects on turbulence. The model demonstrated the ability to qualitatively simulate events when initialized with actual CTD data and forced with a realistic meteorological time series, provided the heat fluxes were adjusted to give a correct total heat loss from the ocean. Further work toward tuning of the model constants  $m_1$ ,  $m_2$ ,  $m_3$ , and  $m_4$ , and the inclusion of a shallowing mode have the prospect of making the model quantitatively useful.

Several conclusions can be made about the mixing that occurred in the Greenland Sea during late winter 1994:

- Horizontal wind-driven energy exceeded vertical free convective energy throughout the period; the turbulence was anisotropic, and wind stirring was dominant over cooling even during a period of strong cooling.

- In the vertical energy budget, pressure redistribution of horizontal energy (from the wind) was a larger source of energy than surface buoyancy flux; free convection was not dominant even when considering  $\overline{w'^2}$  only. This underscores the importance of including wind unsteadiness.
- The deepening response for a given forcing event depends not only upon the strength of the event, but also upon the initial turbulent energy, the depth of the layer, the buoyancy jump at the bottom of the layer, and the stratification below the turbulent region.
- The direction of the wind may be important not only during strong events, but between them as well, because it influences the “spinup” time for the next entraining event.
- The phase of the surface buoyancy flux to shear production also differs among events; it is possible that this difference may influence the storm’s efficiency at deepening the mixed layer.

This study demonstrates the importance of water column initial conditions, the accurate representation of strong surface cooling events, and inclusion of the thermobaric effect on buoyancy to determine the depth of mixing and ultimately the heat and salt flux into the deep ocean.

## **B. RECOMMENDATIONS**

One of the primary motivations for the study of deep mixed layers is to be eventually able to parameterize mixed layer dynamics, in particular the dynamics of deep

mixed layers and subgrid scale penetrative convection. The requirement is that the effects of these processes be included in general circulation models despite the impracticability of modeling the actual physical processes within the general circulation model itself. This research provides a tool for studying various forcing events and their calculated effects, to conceptualize and test what the important variables in such a parameterization might be.

To increase this model's usefulness, several areas need further study:

- Include a shallowing mode capability. Turbulence may be dissipated even without warming, so that the fully turbulent layer may at times be much shallower than the layer that is well-mixed in potential temperature and salinity. The additional time required to re-stir the layer is currently neglected.
- Include a finite thickness entrainment zone. Stability within or across the zone may be important.
- Compare deepening and energy component behavior to results from large eddy simulations of the same events. Specifically, find better estimates of model constants, and ensure the correct amount of anisotropy. This would be an important step to improving the quantitative accuracy of the model.





## LIST OF REFERENCES

- Bourke, R., R. Paquette, and R. Blythe, 1992. The Jan Mayen current of the Greenland Sea. *J. Geophys. Res.*, 97, 7241-7250.
- Brown, R. A., 1970. A secondary flow model for the planetary boundary layer. *J. Atmos. Sci.*, 27, 742-757.
- Brown, W. S., and R. C. Beardsley, 1978. Winter circulation in the western Gulf of Maine: Part 1. Cooling and water mass formation. *J. Phys. Oceanogr.*, 8, 265-277.
- Garwood, R. W., Jr., 1977. An oceanic mixed layer model capable of simulating cyclic states. *J. Phys. Oceanogr.*, 7, 455-468.
- Garwood, R. W., Jr., 1979. Air-sea interaction and dynamics of the surface mixed layer. *Review of Geophysics and Space Physics*, Vol. 17, No. 7, 1507-1524.
- Garwood, R. W., Jr., P. Muller, and P. C. Gallacher, 1985. Wind direction and equilibrium mixed layer depth: General theory. *J. Phys. Oceanogr.*, 15, 1325-1331.
- Garwood, R. W., Jr., 1991. Enhancements to deep turbulent entrainment, In *Deep Convection and Deep Water Formation in the Oceans*, Ed. by P. C. Chu and J.-C. Gascard, 197-213, Elsevier Science.
- Garwood, R. W., Jr., S. M. Isakari, and P. C. Gallacher, 1994. Thermobaric convection, in *The Polar Oceans and Their Role in Shaping the Global Environment*, O. Johannessen, R. Meunch and J. Overland, Eds., Geophysical Monograph 85, 199-209.
- Gascard J.-C., 1973. Vertical motions in a region of deep water formation, *Deep-Sea Research*, 20, 1011-1027.
- Gill, A. E., 1973. Circulation and bottom water formation in the Weddell Sea, *Deep-Sea Res.*, 20, 111-140.
- Gordon, A. L., 1978. Deep Antarctic convection of Maud Rise. *J. Phys. Oceanogr.*, 8, 600-612.
- Killworth, P. D., 1979. On "chimney" formations in the deep ocean. *J. Phys. Oceanogr.*, 9, 531-554.
- Large, W. G., J. C. McWilliams, and S. C. Doney, 1994. Oceanic vertical mixing: A review and a model with a nonlocal boundary layer parameterization. *Rev. Geophys.*, 32, 363-403.

- McDougall, T. J., 1987. Thermobaricity, cabbeling, and water-mass conversion. *J. Geophys. Res.*, 92, 5448-5464.
- Nansen, F., 1906. Northern Waters: Captain Roald Amundsen's observations in the Arctic Seas in 1901. With a discussion of the bottom-waters of the Northern Seas. *Skr. Nor. Vidensk. Akad. Kl. 1:Mat.-Naturvidensk. Kl.*, 3.
- Nansen, F., 1912. Das Bodenwasser und die Abkühlung des Meeres. *Int. Rev., ges. Hydrobiol., Hydrogr.*, Bd. v, 1-32.
- Rossby, C. G., and R. B. Montgomery, 1935. The layer of frictional influence in wind and ocean currents. *Pap. Phys. Oceanogr. Meteor.*, 3, Annual Reviews, 101 pp.
- Rotta, J., 1951. Statische Theorie Nichthomogener Turbulenz, *Z. Physik*, Vol. 129, 547-572.
- Rudels, B., D. Quadfasel, H. Friedrich, and M.-N. Houssais, 1989. Greenland Sea convection in the winter of 1987-1988. *J. Geophys. Res.*, 94, 3223-3227.
- Schott, F., M. Visbeck, and J. Fischer, 1993. Observations of vertical currents and convection in the central Greenland Sea during the winter of 1988/1989. *J. Geophys. Res.*, 98, 14,401-14,421.
- Stull, R. B., 1988. *An introduction to boundary layer meteorology*, p. 478. Dordrecht: Kluwer Academic Publishers.
- Visbeck, M., J. Fischer, and F. Schott, 1995. Preconditioning in the Greenland Sea for deep convection: ice formation and ice drift. *J. Geophys. Res.*, 100, 18,489-18,502.
- Wüst, G., 1928. Der Ursprung der Atlantischen Tiefenwasser, (Aus den Ergebnissen der Deutschen Atlantischen Expedition), Jubiläums-Sonderband 1928 der Zeitschrift der Gesellschaft für Erdkunde zu Berlin, Berlin.
- Wyngaard, J. C., S. P. S. Arya, and O. R. Cote, 1974. Some aspects of the structure of convective boundary layers. *J. Atmos. Sci.*, 31, 747-754.
- Zilitinkevich, S. S., D. V. Chalikov and Yu. D. Resnyansky, 1979. Modeling the oceanic upper layer. *Oceanol. Acta.*, 2, 219-240.

## INITIAL DISTRIBUTION LIST

	No. Copies
1. Defense Technical Information Center ..... 8725 John J. Kingman Rd., Ste 0944 Ft. Belvoir, VA 22060-6218	2
2. Dudley Knox Library ..... Naval Postgraduate School 411 Dyer Rd. Monterey, CA 93943-5101	2
3. Chairman(Code OC/BF) ..... Department of Oceanography Naval Postgraduate School Monterey, CA 93943-5101	1
4. Chairman(Code MR/Wx) ..... Department of Meteorology Naval Postgraduate School Monterey, CA 93943-5101	1
5. Prof. Roland W. Garwood ..... Department of Oceanography Naval Postgraduate School Monterey, CA 93943-5101	2
6. Prof. Peter S. Guest ..... Department of Meteorology Naval Postgraduate School Monterey, CA 93943-5101	1
7. Mr. Ramsey Harcourt ..... Department of Oceanography Naval Postgraduate School Monterey, CA 93943-5101	1
8. Prof. Albert J. Semtner ..... Department of Oceanography Naval Postgraduate School Monterey, CA 93943-5101	1

9. Prof. Wieslaw Maslowski ..... 1  
Department of Oceanography  
Naval Postgraduate School  
Monterey, CA 93943-5101
10. Prof. Ching-Sang Chiu ..... 1  
Department of Oceanography  
Naval Postgraduate School  
Monterey, CA 93943-5101
11. Prof. Lin Jiang ..... 1  
Department of Oceanography  
Naval Postgraduate School  
Monterey, CA 93943-5101
12. Mme. Pascale Lherminier ..... 1  
LODYC, tour 14, 2e etage, case 100  
Universite Pierre et Marie Curie  
4, Place Jussieu  
75252 Paris Cedex 05  
FRANCE
13. Office of Naval Research ..... 1  
800 North Quincy Street, Ballston Tower One  
Arlington, VA 22217-5660
14. Office of Naval Research ..... 1  
Code 322OM  
ATTN: Dr. Manual Fiadeiro  
800 North Quincy Street  
Arlington, VA 22217-5660
15. Office of Naval Research ..... 1  
Code 322PO  
ATTN: Dr. Steve Ramp  
800 North Quincy Street  
Arlington, VA 22217-5660
16. Mr. Alan Hayashida ..... 1  
NUWC DET Arctic Submarine Laboratory  
48750 Fleming Rd.  
San Diego, CA 92152-7210

17. National Science Foundation ..... 1  
Office of Polar Programs  
ATTN: Dr. Odile De La Beaujardiere  
4201 Wilson Blvd.  
Arlington, VA 22230
18. LCDR Rebecca E. Stone ..... 2  
104 Leidig Circle  
Monterey, CA 93940